Mechanisms of Chromosome Positioning During Mitosis

Ivan Sigmund,[1] Domagoj Božan,[1] Ivana Šarić,[2] and Nenad Pavin[1]
[1]*Physics Department, Faculty of Science, University of Zagreb, Bijenika cesta 32, 10 000 Zagreb, Croatia*
[2]*Ruđer Bošković Institute, Bijenička Cesta 54, 10000 Zagreb, Croatia*

(Received 10 May 2024; accepted 12 November 2024; published 5 December 2024)

The mitotic spindle, a micromachine composed of microtubules and associated proteins, plays a pivotal role in ensuring the accurate segregation of chromosomes. During spindle assembly, initially randomly distributed chromosomes are transported toward the equatorial plate and experiments suggest that several competing mechanisms can contribute to this process of chromosome congression. However, a systematic theoretical study of forces relevant to chromosome congression is still lacking. Here we show, by introducing a physical model, that length-dependent forces generated by motor proteins transport chromosomes toward the spindle equator. Passive cross-linkers, on the other hand, can generate off-centering forces that impair chromosome congression. Our mean-field approach also reveals that stable points can exist in the vicinity of spindle poles, in addition to the one in the center, and thus provides an explanation for erroneous spindles with polar chromosomes. Taking all these processes into account, our study provides a comprehensive approach to understanding how different spindle components interact with each other and generate forces that drive chromosome congression.

DOI: 10.1103/PRXLife.2.043017

I. INTRODUCTION

The ability of the cell to replicate itself by cell division is one of the basic principles of life. To ensure proper segregation of duplicated genetic material between two daughter cells, the cell arranges chromosomes in space and time. At the beginning of mitosis, the cell exerts forces that transport the chromosomes from initial random positions toward the future division plane in a process termed congression [1–5], as depicted in Fig. 1. Once congression is completed and chromosomes are aligned with the metaphase plane, mitosis proceeds by initiating the segregation of chromosomes. Thus, a precise coordination of forces in space and time is required for the arrangement of chromosomes during cell division.

The mitotic spindle is a bipolar micromachine composed of microtubules (MTs) and associated proteins that self-assembles at the beginning of mitosis and generates the forces responsible for the chromosome positioning [5–8]. Spindle assembly relies on dynamic properties of MTs, including polymerization, depolymerization, and stochastic transitions between these two states [9]. Spindle MTs can extend from spindle poles and interact with chromosomes via kinetochores, termed kinetochore MTs [10]. Spindle MTs that extend from opposite poles and interdigitate, enabling motor and nonmotor proteins to cross-link them, and thus perform various biological functions [11–17], are termed nonkinetochore MTs. These interactions between MTs and chromosomes, mediated by motor proteins, drive chromosome congression.

Forces directed toward the spindle midplane are crucial for chromosome assembly, and various mechanisms have been proposed to explain how these forces arise [18]. Experiments show that MTs extending from poles exert a force that pushes chromosomes away from the pole, known as polar ejection force, and that this force is generated by motor proteins at chromosome arms [19–22]. Forces oriented toward the spindle midplane are also exerted by plus-end-directed motor proteins at kinetochores, such as CENP-E/kinesin-7, which move along nonkinetochore MTs [23,24]. A recent study has shown that chromosome congression relies on end-on kinetochore-MT attachments and in their absence, chromosomes do not congress [25]. Pulling forces on kinetochores are generated by depolymerization of end-on attached MTs, as shown *in vitro* and *in vivo* [26–29]. Because forces at sister kinetochores are oriented toward opposite spindle poles, the force toward the center in this tug-of-war situation is generated when longer MTs exert greater forces than the shorter ones. The MT length-dependent forces are produced by the accumulation of a greater number of kinesin-8 motor proteins at the plus end, where they promote MT depolymerization and consequently increase pulling forces at the kinetochore to which they are attached [30–33]. Alternatively, the longer MT can also generate greater force through motor proteins that accumulate along it in a length-dependent manner and generate faster poleward flux [34]. All these studies suggest that different mechanisms contribute to chromosome congression at the same time.

Theoretical models that describe spindle mechanics give quantitative insights into key processes of mitosis. An important process relevant to mitosis is the formation and stability maintenance of antiparallel MT bundles, which have been studied for a pair of antiparallel MTs [35,36], as well as for MTs emanating from two poles or along preexisting MTs [37,38]. Models for spindle formation also rely on MT

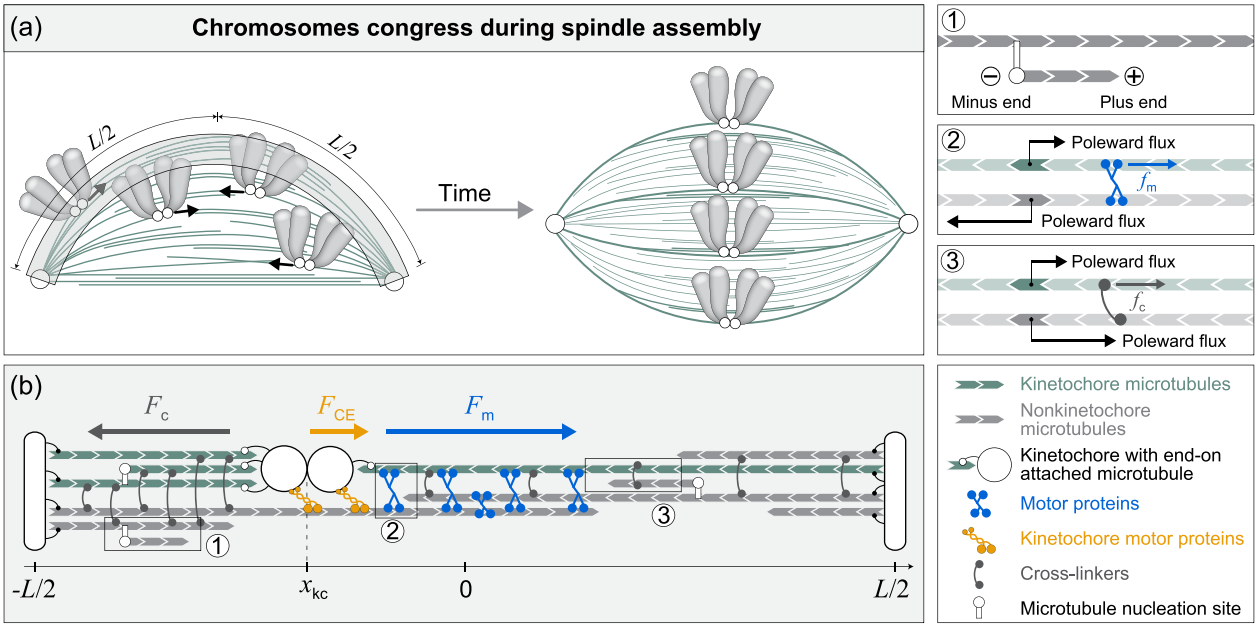

FIG. 1. Model for chromosome congression. (a) Schematic representation of chromosome congression during spindle assembly, where the chromosomes move from initial random positions (left scheme) to the spindle equator (right scheme). MTs (green lines) extend between spindle poles (white circles) and interact with kinetochores (white circles at the chromosomes). Arrows represent chromosome movement direction. (b) Geometry of the one-dimensional model with the spindle center at location $x = 0$, two poles at locations $-L/2$ and $L/2$, and kinetochores at x_{kc}. MTs are attached to kinetochores or not. They extend from spindle poles or nucleation sites at preexisting MTs. Motor proteins link antiparallel MTs and exert force F_m, while passive cross-linkers link parallel MTs and exert force F_c on the kinetochores. Kinetochore motor proteins link kinetochores to MTs, exerting force F_{CE}. Individual parts of the scheme are explained in the legend on the right. Inset 1 shows an enlarged segment showing the MT nucleated along a preexisting MT. The more dynamic plus end is denoted by a plus sign and the less dynamic minus end is denoted by a minus sign. Inset 2 shows the motor protein linking kinetochore MT with its antiparallel neighbor and exerting force f_m on the kinetochore MT. The arrows denote the direction of poleward flux of respective MTs. Inset 3 shows a passive cross-linker linking the kinetochore MT with its parallel neighbor and exerting the force f_c on the kinetochore MT. The arrows denote the direction of poleward flux of respective MTs.

reorientation that leads to MT alignment, which is driven by motor proteins and passive cross-linkers [39,40]. Several theoretical models have studied how MTs and kinetochores explore the space to get into the proximity of each other and subsequently form kinetochore-MT attachments, including biorientation [41–47]. In order to study chromosome positioning, in yeasts the models explored the contribution of length- and tension-dependent regulation of MT dynamics [48–52], whereas in higher eukaryotes the models incorporate polar ejection forces and forces generated by kinetochore motor proteins [53–57]. Recently, we showed that length-dependent MT poleward flux generates centering forces at the kinetochores during metaphase [34]. However, important mechanisms that could drive chromosome congression, such as MT length-dependent force and its cooperation with kinetochore motor proteins, have not been explored so far.

In this paper, we introduce a one-dimensional model describing forces that drive chromosome congression in human spindles. These forces are generated by motor proteins and passive cross-linkers that are attached to kinetochore MTs and drive the poleward flux of these MTs. To determine the numbers of motor proteins and cross-linkers, we calculate MT distributions from their dynamic properties. The key process behind the centering mechanism is the competition between length-dependent pulling forces and the number of MTs that attach to kinetochores. By using parameters that are relevant for human cells, we find that motor proteins lead to congression times comparable to experimentally measured values. Passive cross-linkers, on the other hand, can generate off-centering forces that impair chromosome congression, but in competition with motor forces, they are weaker and do not affect centering. Kinetochore-associated motor proteins generate a centering force that works together with these forces. Thus, our theory presents a methodical framework for understanding the interactions among diverse spindle components and the forces they generate to transport chromosomes during spindle assembly.

II. MODEL

In order to study chromosome congression, we introduce a one-dimensional model that describes the distribution of MTs and the forces that arise in the interaction of MTs with kinetochores (Fig. 1). These forces are caused by the flux of MTs, which depends on the length of the MTs, as a consequence of the accumulation of motor proteins, such as Eg5/kinesin-5 [58–60], and cross-linker proteins, such as NuMA [61], on the MTs. The model also includes forces generated by plus-end-directed kinetochore motor proteins, such as CENP-E. The key part of our model is MT length-dependent force, where longer overlaps of antiparallel MTs accumulate a greater number of motor proteins. For this reason, longer MTs that are

attached to the kinetochore from the farther pole side will generate a greater force than those from the near pole side, thus centering the chromosome.

In order to evaluate this force, we need to calculate the distributions of MTs. Because MTs in human spindles are predominantly aligned with each other [8], we use a one-dimensional approach in which we consider MT distributions with respect to the line parallel to the MTs. We separately consider the MTs that are attached to kinetochores and those that are not, where each of them is extending from the pole or preexisting MTs. In addition, MTs that are not attached to kinetochores are growing or pausing. Because MT distributions are dynamically generated, we calculate them by taking into account known MT properties, including nucleation, growth, pausing, and catastrophe.

A. Forces relevant for chromosome congression

In our one-dimensional approach, the position along the spindle is denoted by x and can take values between $-L/2$ and $L/2$, representing the left and right poles, respectively (Fig. 1). Furthermore, $x = 0$ denotes the position of the spindle center. To calculate how the position of the center of mass of the sister kinetochores $x_{\rm kc}$ changes in time t, we consider the force balance at the kinetochores:

$$\eta \frac{{\rm d}x_{\rm kc}}{{\rm d}t} = F_\ell + F_{\rm r}. \tag{1}$$

Here η denotes the cytoplasmic drag friction coefficient of the chromosome and $F_{\ell,{\rm r}}$ denotes the forces at the kinetochore. The indices ℓ and r denote the left and right sister kinetochores, respectively.

Forces on the kinetochores arise from the MT plus-end interaction with the kinetochores or from the interaction with kinetochore motor proteins that link kinetochores to MTs laterally,

$$F_{\rm r} = F_{\rm kMT} + F_{\rm CE}. \tag{2}$$

Here the interaction between the right kinetochore and $N_{\rm k}$ MTs attached to it is calculated as $F_{\rm kMT} = \sum_{i=1}^{N_{\rm k}} (F_{\rm m}^i + F_{\rm c}^i)$. The forces exerted by motor proteins and cross-linkers on the ith kinetochore MT are denoted by $F_{\rm m}^i$ and $F_{\rm c}^i$, respectively. The force exerted by kinetochore motor proteins is denoted $F_{\rm CE}$. Note that here and in the rest of this section we consider forces exerted on the right-hand side only, whereas the complete description of the model is provided in Appendix A.

The forces exerted by motor proteins and cross-linkers attached to the ith kinetochore MT are given as

$$F_{\rm m,c}^i = m_{\rm m,c}^i f_{\rm m,c}^i. \tag{3}$$

Here the numbers of motor proteins and cross-linkers are denoted by $m_{\rm m}^i$, and $m_{\rm c}^i$, respectively. The average forces exerted by these motor proteins and cross-linkers are denoted by $f_{\rm m}^i$ and $f_{\rm c}^i$, respectively. We calculate the numbers of motor proteins and cross-linkers attached to the ith kinetochore MT of length l^i as

$$m_{\rm m,c}^i = \int_{x_{\rm kc}}^{x_{\rm kc}+l^i} dx\, c_{\rm m,c} P_{\rm ap,pp}(x), \tag{4}$$

where the integration limits, and consequently the numbers of motor proteins and cross-linkers, depend on the kinetochore position. Here we take into account that the distribution of motor proteins and cross-linkers depends on the probability of binding to antiparallel neighboring MTs $P_{\rm ap}(x)$ and parallel neighboring MT $P_{\rm pp}(x)$, respectively. Linear densities of motor proteins and cross-linkers are denoted by $c_{\rm m}$ and $c_{\rm c}$, respectively. The fraction of motor proteins that bind to the kinetochore MT and a neighboring antiparallel MT is proportional to the probability of finding an antiparallel neighbor at that position, $P_{\rm ap}(x) = \frac{N_\ell(x)}{N_\ell(x)+N_{\rm r}(x)}$. Similarly, the fraction of passive cross-linkers that bind to the kinetochore MT and a neighboring parallel MT is proportional to the probability of finding a parallel neighbor at that position, $P_{\rm pp}(x) = \frac{N_{\rm r}(x)}{N_\ell(x)+N_{\rm r}(x)}$. Here N_ℓ and $N_{\rm r}$ denote the numbers of left and right nonkinetochore MTs, respectively. We also define the lengths of parallel and antiparallel overlaps with kinetochore MTs of length l^i as $l_{\rm ap,pp}^i \equiv \int_{x_{\rm kc}}^{x_{\rm kc}+l^i} dx\, P_{\rm ap,pp}(x)$. As linear densities of motor proteins and cross-linkers are constant, Eq. (4) simplifies to $m_{\rm m,c}^i = c_{\rm m,c}\, l_{\rm ap,pp}^i$. By using these overlap lengths, we calculate the average overlaps for the kinetochore-MT bundle composed of $N_{\rm k}$ MTs as

$$L_{\rm pp,ap} \equiv \frac{1}{N_k} \sum_{i=1}^{N_{\rm k}} l_{\rm pp,ap}^i. \tag{5}$$

We calculate the velocity of motor proteins from the force-velocity relationship $v_{\rm m} = v_0(1 - f_{\rm m}/f_0)$. Here $f_{\rm m}$ is a load force that opposes motor movement, f_0 is the stall force of the motor, and v_0 is the velocity of the motor protein without a load. The motor velocity is equal to the relative sliding velocity of antiparallel MTs, where $v_{\rm m} = v_{\rm kf}^i - v_{{\rm f}\ell}$ describes the case in which kinetochore MT and the associated nonkinetochore MT have poleward fluxes $v_{\rm kf}^i$ and $v_{{\rm f}\ell}$, respectively. On the other hand, cross-linkers cannot generate an active force between MTs, but if MTs slide between each other, the cross-linkers oppose this movement by exerting a damping force. In our model, the damping force of a cross-linker that connects parallel MTs is given as $f_{\rm c} = -\xi_{\rm c} v_{\rm c}$, where $\xi_{\rm c}$ denotes the viscous friction coefficient. The relative sliding velocity of the kinetochore MT and the associated nonkinetochore parallel MT is given as $v_{\rm c} = v_{\rm kf}^i - v_{\rm fr}$.

In order to quantify the forces on the kinetochore MTs, we impose that all kinetochore MTs of the same bundle slide with the same velocity $v_{\rm kf}^i = v_{\rm kf}$ and consequently all the forces in the same bundle have the same value $f_{\rm m,c}^i = f_{\rm m,c}$. This constraint, which dramatically reduces the number of unknowns, is plausible because MTs within the same kinetochore-MT bundle are connected by passive cross-linking proteins. In this limit, the force between the MTs and the kinetochore simplifies to

$$F_{\rm kMT} = M_{\rm m} f_{\rm m} + M_{\rm c} f_{\rm c}. \tag{6}$$

The number of motor proteins and cross-linkers on the kinetochore-MT bundle is given as $M_{\rm m,c} = \sum_{i=1}^{N_{\rm k}} m_{\rm m,c}^i$, which in combination with Eqs. (4) and (5) yields

$$M_{\rm m,c} = c_{\rm m,c} N_{\rm k} L_{\rm ap,pp}. \tag{7}$$

This equation is the core of the length-dependent force at the kinetochore. Note that the average overlap lengths depend on the position of the kinetochore, which in turn affects its positioning. We also use a constant flux velocity for nonkinetochore MTs, $v_{f\ell,\mathrm{fr}} = \mp v_0/2$, based on results from [34].

The interaction between a kinetochore and the MTs attached to it is given by a relationship between the pulling force exerted by the kinetochore and the growth velocity of the MTs [62]. We simplify this relationship with a linear expression $v_{\mathrm{gk}} = \frac{1}{\xi_{\mathrm{gk}}} F_{\mathrm{kMT}}$. Here the growth velocity of the kinetochore MTs v_{gk} is calculated from the relative movement of kinetochore MTs, which flux with the poleward velocity v_{kf}, with respect to the kinetochore, which moves with velocity $v_{\mathrm{kc}} \equiv dx_{\mathrm{kc}}/dt$, resulting in $v_{\mathrm{gk}} = v_{\mathrm{kf}} - v_{\mathrm{kc}}$. The effective friction coefficient is denoted by ξ_{gk}.

The model also includes kinetochore motor proteins which exert forces by moving along nonkinetochore MTs in a plus-end-directed manner. We describe the force exerted by N_{CE} kinetochore motor proteins as

$$F_{\mathrm{CE}} = N_{\mathrm{CE}}[f_{\mathrm{CE,pp}} P_{\mathrm{pp}}(x_{\mathrm{kc}}) + f_{\mathrm{CE,ap}} P_{\mathrm{ap}}(x_{\mathrm{kc}})], \tag{8}$$

where the direction and magnitude of the forces exerted by kinetochore motor proteins depend on MT orientation. For the right sister kinetochore, described by Eq. (8), the forces exerted toward the left and right by kinetochore motor proteins are denoted by $f_{\mathrm{CE,pp}}$ and $f_{\mathrm{CE,ap}}$, respectively. These forces are calculated from the force velocity relationships $v_{\mathrm{CE,pp}} = v_{\mathrm{CE0}}(-1 - \frac{f_{\mathrm{CE,pp}}}{f_{\mathrm{CE0}}})$ and $v_{\mathrm{CE,ap}} = v_{\mathrm{CE0}}(1 - \frac{f_{\mathrm{CE,ap}}}{f_{\mathrm{CE0}}})$. The velocity of kinetochore motor proteins is calculated as the relative velocity of the kinetochore with respect to the associated nonkinetochore MT, $v_{\mathrm{CE,pp}} = (v_{\mathrm{kc}} - v_{\mathrm{fr}})$ and $v_{\mathrm{CE,ap}} = (v_{\mathrm{kc}} - v_{f\ell})$. Here f_{CE0} denotes the stall force of the kinetochore motor proteins and v_{CE0} the velocity without a load.

B. Distributions of kinetochore and nonkinetochore microtubules

In order to calculate the number of MTs, the overlap lengths, and the probabilities $P_{\mathrm{ap,pp}}$ used in Eqs. (7) and (8), we need to evaluate the MT distributions, which we obtain using a mean-field approach. This approach neglects fluctuations and thus it is suitable for systems with a large number of MTs. In our case, it is adequate for the description of nonkinetochore MTs, whose number in the metaphase is around 5000, whereas it provides an estimate for kinetochore MTs, whose number is around 10, as measured in Ref. [8]. For these reasons, the mean-field approach is relevant for describing typical kinetochore movement, whereas stochastic simulations are more appropriate for studying the variability in the movement of individual kinetochores, as in Refs. [46,47,57].

Our model describes growing and pausing MTs, nucleated either on the pole or along preexisting MTs. The densities of these four distributions are denoted by $n_{\mathrm{p}}(l)$, $\tilde{n}_{\mathrm{p}}(l)$, $\rho_{\mathrm{n}}(l,x)$, and $\tilde{\rho}_{\mathrm{n}}(l,x)$, respectively. These densities determine the number of MTs of length l extending from the pole, $dN_{\mathrm{p}} = (n_{\mathrm{p}} + \tilde{n}_{\mathrm{p}})dl$, and the number of MTs of length l extending from a nucleation site at position x, $dN_n = (\rho_{\mathrm{n}} + \tilde{\rho}_{\mathrm{n}})dldx$. Following approaches from previous studies [63–65], the MT densities are calculated from their dynamic properties using transport equations. For MTs that extend from the pole, the equations are

$$\frac{\partial n_{\mathrm{p}}}{\partial t} = k_{\mathrm{p}}\delta(l) - k_{\mathrm{ps}} n_{\mathrm{p}} - v_{\mathrm{g}} \frac{\partial n_{\mathrm{p}}}{\partial l}, \tag{9}$$

$$\frac{\partial \tilde{n}_{\mathrm{p}}}{\partial t} = k_{\mathrm{ps}} n_{\mathrm{p}} - k_{\mathrm{cat}} \tilde{n}_{\mathrm{p}}, \tag{10}$$

and for those that extend from preexisting MTs, the equations are

$$\frac{\partial \rho_{\mathrm{n}}}{\partial t} = k_{\mathrm{n}} c\delta(l) N_{\mathrm{p}}(x) - k_{\mathrm{ps}}\rho_{\mathrm{n}} - v_{\mathrm{g}} \frac{\partial \rho_{\mathrm{n}}}{\partial l}, \tag{11}$$

$$\frac{\partial \tilde{\rho}_{\mathrm{n}}}{\partial t} = k_{\mathrm{ps}}\rho_{\mathrm{n}} - k_{\mathrm{cat}}\tilde{\rho}_{\mathrm{n}}. \tag{12}$$

In Eq. (9) the first term on the right-hand side describes MT nucleation at the pole that occurs with rate k_{p}, where the Dirac delta function $\delta(l)$ ensures that nucleated MTs have zero length. The second term describes the MT switch from growing to pausing, which occurs at a rate k_{ps}. The last term describes MT growth, in which the drift velocity is an effective MT growth velocity v_{g}. The pausing MTs extending from the pole are described by Eq. (10) and they disappear upon catastrophe with a rate k_{cat}. The number of preexisting MTs extending from the pole includes pausing and growing MTs and it is calculated as $N_{\mathrm{p}}(x) = \int_{L/2-x}^{\infty} dl\, n_{\mathrm{p}}(l) + \tilde{n}_{\mathrm{p}}(l)$. In Eq. (11) the first term describes MT nucleation along preexisting MTs extending from the pole with nucleation rate multiplied by the density of nucleation sites along a single MT, $k_{\mathrm{n}}c$. The pausing MTs nucleated along preexisting MTs are described by Eq. (12).

Growing MTs can attach to kinetochores when the MT plus end is close to the kinetochore. The number of kinetochore MTs extending from the pole is calculated as

$$\frac{\mathrm{d}N_{\mathrm{kp}}}{\mathrm{d}t} = (v_{\mathrm{kc}} + v_{\mathrm{g}}) n_{\mathrm{p}}|_{l=L/2-x_{\mathrm{kc}}} p_{\mathrm{att}} \left(1 - \frac{N_{\mathrm{k}}}{N_0}\right) - k_{\mathrm{off}} N_{\mathrm{kp}}, \tag{13}$$

whereas the density of kinetochore MTs nucleated along preexisting MTs is a function of MT length and is calculated as

$$\frac{\partial n_{\mathrm{kn}}}{\partial t} = (v_{\mathrm{kc}} + v_{\mathrm{g}}) \rho_{\mathrm{n}}|_{x=l+x_{\mathrm{kc}}} p_{\mathrm{att}} \left(1 - \frac{N_{\mathrm{k}}}{N_0}\right) - k_{\mathrm{off}} n_{\mathrm{kn}}. \tag{14}$$

In these two equations, the first term on the right-hand side is the rate of MT attachment to kinetochores, which is proportional to the current of MT plus ends at the kinetochore position. The current is calculated as the velocity of the MT plus ends with respect to the kinetochore multiplied by the density of plus ends of nonkinetochore MTs. The attachment probability to an unoccupied kinetochore site is denoted by p_{att}. A fraction of unoccupied attachment sites is calculated as the number of unoccupied attachment sites $N_0 - N_{\mathrm{k}}$ divided by the number of attachment sites N_0. Microtubules detach from kinetochores at a rate k_{off}.

The number of kinetochore MTs is given as

$$N_{\mathrm{k}} = N_{\mathrm{kp}} + N_{\mathrm{kn}}(x_{\mathrm{kc}}), \tag{15}$$

where the number of kinetochore MTs nucleated along preexisting MTs and reaching position x is calculated as

$$N_{\rm kn}(x) = \int_{x-x_{\rm kc}}^{L/2-x_{\rm kc}} n_{\rm kn} dl, \tag{16}$$

which is valid for x between $x_{\rm kc}$ and $L/2$. The overlap lengths $L_{\rm ap}$ and $L_{\rm pp}$ are calculated as

$$L_{\rm ap,pp} = \frac{1}{N_{\rm k}}\left(N_{\rm kp}\int_{x_{\rm kc}}^{L/2} dx\, P_{\ell,{\rm r}} + \int_0^{L/2-x_{\rm kc}} dl\, n_{\rm kn}\int_{x_{\rm kc}}^{x_{\rm kc}+l} dx P_{\ell,{\rm r}}\right). \tag{17}$$

In this mean-field approach, the sum over individual kinetochore MTs from Eq. (5) is split into two parts. The first part describes kinetochore MTs that extend from the pole to the kinetochore and all have the same length. The second part of the sum describes kinetochore MTs nucleated along preexisting MTs.

In this section, we have presented a one-dimensional model for chromosome congression, which includes MT dynamics and forces exerted by motor proteins, cross-linkers, and kinetochore motor proteins. We aim to calculate the kinetochore velocity $v_{\rm kc}$ as it is a key indicator of the vitality of the congression and the stability of the metaphase plate. Using the equations for the balance of forces on the kinetochores [Eqs. (1) and (2)] together with the expressions for kinetochore-MT growth velocities [Eq. (A5)], average motor protein forces [Eq. (A6)], average cross-linker forces [Eq. (A7)], and average kinetochore-motor-protein forces [Eq. (A8)], we can calculate the kinetochore velocity $v_{\rm kc}$ as provided in Appendix B. The resulting formula for the kinetochore velocity as a function of the numbers of motor proteins, cross-linkers, and kinetochore motor proteins is

$$v_{\rm kc} = \frac{v_0}{2\gamma_{\rm MT}}\left(\frac{f_0}{v_0}(M_{\rm mr}-M_{{\rm m}\ell}) + \xi_{\rm c}(M_{\rm cr}-M_{{\rm c}\ell})\right) + \frac{v_{\rm CE0}-v_0/2}{\gamma_{\rm CE}}\frac{f_{\rm CE0}}{v_{\rm CE0}}2N_{\rm CE}(P_\ell - P_{\rm r}). \tag{18}$$

Here $\gamma_{\rm MT} \equiv (\eta + 2N_{\rm CE}\frac{f_{\rm CE0}}{v_{\rm CE0}})(1+\frac{\beta_r}{\xi_{gk}})(1+\frac{\beta_\ell}{\xi_{gk}}) + [\frac{f_0}{v_0}(M_{\rm mr}+M_{{\rm m}\ell}) + \xi_{\rm c}(M_{\rm cr}+M_{{\rm c}\ell}) + 2\frac{\beta_r\beta_\ell}{\xi_{\rm gk}}]$ is a shorthand notation for a positive function of $x_{\rm kc}$ and it represents an effective drag coefficient for the interaction between MTs and the kinetochore. The shorthand notation $\beta_{{\rm r},\ell} \equiv M_{{\rm mr},\ell}\frac{f_0}{v_0} + M_{{\rm cr},\ell}\xi_{\rm c}$ is the sum of motor proteins and cross-linkers on the right or left side, respectively. The shorthand notation for the effective drag coefficient from the interactions between the kinetochores and the kinetochore motor proteins is $\gamma_{\rm CE} \equiv \gamma_{\rm MT}/(1+\frac{\beta_r}{\xi_{\rm gk}})(1+\frac{\beta_\ell}{\xi_{\rm gk}})$. Furthermore, $P_{\rm pp}$ and $P_{\rm ap}$ have been replaced with $P_{\rm l} \equiv \frac{N_{\rm l}(x)}{N_\ell(x)+N_{\rm r}(x)}$ and $P_{\rm r} \equiv \frac{N_{\rm r}(x)}{N_\ell(x)+N_{\rm r}(x)}$, since the same equations describe kinetochore motor proteins on both kinetochores. The terms in parentheses in Eq. (18) show that the direction of the velocity is dictated by the differences in the total number of motor proteins, cross-linkers, and kinetochore motor proteins on the right and left side, each contributing to the velocity with different magnitudes.

III. RESULTS

In our model, the movements of the kinetochores are governed by a combination of forces exerted by motor proteins and passive cross-linkers on the kinetochore MTs, as well as kinetochore motor proteins [see Eq. (18)]. Additionally, the distributions of these proteins depend on the geometry of the system, including the number of MTs and their average length, and thus getting a deeper insight into the contributions of different proteins is challenging. Therefore, we study the contributions of each protein separately, as well as concurrently. In this way, we gain a comprehensive understanding of how they work together to ensure proper chromosome congression.

We solve the MT distribution equations in a steady-state limit (see Appendix C), which is reasonable due to the difference in timescales. For nonkinetochore MTs, the MT growth time $k_{\rm ps}^{-1} \approx 0.1$ min is much shorter than the time needed for congression, usually 5–10 min [25,66]. We also calculate the kinetochore-MT distributions in a steady-state limit (see Appendix D), because the kinetochore-MT detachment time $k_{\rm off}^{-1} \approx 3.5$ min [67] is shorter than the congression time. We selected the model parameters based on recent *in vitro* and *in vivo* measurements. Table I shows the MT and kinetochore parameters, and Table II shows the motor protein, cross-linker, and kinetochore-motor-protein-related parameters.

A. Motor proteins exert length-dependent forces that drive chromosome congression

In order to explore whether motor proteins can generate forces that drive chromosome congression, we reduce our model by setting the number of passive cross-linkers and kinetochore motor proteins to zero. In this regime we recalculate Eq. (18), which then simplifies to

$$\frac{dx_{\rm kc}}{dt} = \frac{v_0}{2}\frac{\frac{M_{\rm mr}}{M_{{\rm m}\ell}}-1}{\frac{M_{\rm mr}}{M_{{\rm m}\ell}}+1}\left[1 + \frac{\eta v_0}{f_0} + \frac{\eta\xi_{\rm gk}v_0^2}{f_0^2(M_{\rm mr}+M_{{\rm m}\ell})} + \left(2\frac{f_0}{v_0\xi_{\rm gk}} + \frac{\eta}{\xi_{\rm gk}}\right)\frac{M_{\rm mr}M_{{\rm m}\ell}}{M_{\rm mr}+M_{{\rm m}\ell}}\right]^{-1}. \tag{19}$$

Here it is evident that the kinetochore can move with velocity up to $v_0/2$ and that the kinetochore moves toward the side with a larger number of motor proteins. We solve our model by numerically integrating Eq. (19), in which the number of motor proteins is calculated from Eqs. (7), (15), and (17).

For parameters relevant for human spindles (Tables I and II), the kinetochore, which was initially at a position close to the left pole, moves away from it and approaches the spindle equator zone in approximately 4 min [Fig. 2(a)]. Based on this graph, we also estimate that the average velocity is about 1 μm/min. These predictions are consistent with the observed congression time, when compared with central chromosomes (Fig. 3(f) in Ref. [66]), as well as measured kinetochore velocity [25]. The quantitative agreement between theory and experiments suggests that the length-dependent forces generated by motor proteins can drive chromosome congression.

Kinetochore movement is driven by motor proteins that accumulate in greater numbers on the farther pole side than on the closer one [Fig. 2(a), blue lines]. Because the number of

TABLE I. Microtubule and kinetochore parameters.

Parameter	Value	Description
L	12 μm	Pole to pole distance[a]
l_0	2.6 μm	MT length[b]
k_{ps}	11 min^{-1}	MT pause rate[c]
v_g	$k_{ps}l_0 \approx 28$ μm/min	MT growth velocity
k_{cat}	0.6 min^{-1}	MT catastrophe rate[d]
k_p	600 min^{-1}	MT nucleation at poles[e,f]
$k_n c$	0.5 (μm $min)^{-1}$	MT nucleation along MTs[g]
N_0	15	Maximum number of kMTs[h]
p_{att}	0.02	kMT attachment probability[f,i]
k_{off}	0.35 min^{-1}	kMT detachment rate[j]
ξ_{gk}	300 pN min /μm	Effective friction coefficient[k]
η	0.08 pN min /μm	Cytoplasmic drag[l]

[a]From Ref. [68].
[b]Estimated using electron microscopy data [8], which measured a spindle length of 9.48 μm and average nonkinetochore-MT length of 2.07 μm. By scaling to spindle length of 12 μm, we calculate an average MT length of 2.6 μm $\approx$ 2.07 μm $\times \frac{12\ \mu m}{9.48\ \mu m}$.
[c]Calculated by dividing the MT growth velocity from Ref. [69] by the average MT length $k_{ps} \approx \frac{28\ \mu m/min}{2.6\ \mu m}$.
[d] Based on electron microscopy data [8] that counted around 5400 nonkinetochore MTs in a cell and EB1 measurements [69] that counted 62 869 dots in 75 frames for MTs in three cells, giving an estimate of 280 growing MTs. Now, using the steady-state relationship between growing and pausing MTs from Eqs. (C8) and (C9), we calculate $k_{cat} = k_{ps}\frac{280}{5400-280}$.
[e]Calculated using experimental data from Ref. [69]. Out of 280 growing MTs, 65% of the MT tracks in prometaphase are pointing toward the opposite pole and 30% of MT tracks originate from zones up to 1.5 μm away from the poles that can be ascribed to MTs nucleated at the pole. Consequently, the nucleation rate at the pole can be calculated from the estimate of the number of growing MTs nucleated at the pole as $\frac{k_p}{k_{ps}} = 280 \times 0.65 \times 0.30 = 54.6$, from which we calculate k_p.
[f]Note that the parameters k_p and p_{att} are relevant for the one-dimensional model but should be adjusted for more complex geometries.
[g]Calculated using experimental data from Ref. [69] where the number of MTs nucleated along preexisting MTs growing toward opposite poles is $280 \times 0.65 \times 0.7 = 127.4$. Using the parameters of our model, we can estimate the number of growing MTs nucleated along one MT as $\frac{l_0}{k_{ps}}k_n c$ and multiplying by the number of pole MTs gives $N_p\frac{l_0}{k_{ps}}k_n c = 127.4$, where $N_p = \frac{k_p}{k_{cat}} + \frac{k_p}{k_{ps}}$.
[h]From Ref. [70].
[i]Estimated as the ratio of the kinetochore area [47] to the cross-section area of the spindle [68].
[j]From Ref. [67].
[k]Estimated as force at the kinetochore, 300 pN [17], divided by the growth velocity of kinetochore MTs, 1 μm/min [34].
[l]From Ref. [71].

TABLE II. Motor protein and cross-linker parameters. Here KC denotes kinetochore.

Parameter	Value	Description
c_m	10 μm^{-1}	Motor protein concentration[a]
f_0	5 pN	Motor protein stall force[b]
v_0	4 μm/min	Motor protein velocity[c]
c_c	20 μm^{-1}	Cross-linker concentration[a]
ξ_c	0.05 pN min /μm	Cross-linker effective drag[a]
N_{CE}	20	No. of motors at the KC[d]
f_{CE0}	6 pN	KC motor stall force[e]
v_{CE0}	2.4 μm/ min	KC motor velocity[a]

[a]Estimated.
[b]From Ref. [72].
[c]From Ref. [34].
[d]From Ref. [73].
[e]From Ref. [74].

motor proteins depends on antiparallel MT overlaps, we plot the distributions of kinetochore and nonkinetochore MTs for kinetochores at the initial position $x_{kc} = -5$ μm [Fig. 2(b)]. Our calculations show that the number of kinetochore MTs increases linearly with proximity to the kinetochore. By comparing the left and right kinetochore-MT distributions, we find that there are more kinetochore MTs on the closer pole side than on the farther one. The number of nonkinetochore MTs has a maximum in the vicinity of the respective pole and decreases in farther positions. By visualizing the fraction of nonkinetochore MTs that form antiparallel overlaps with kinetochore MTs, it can be seen that there is a substantially larger overlap region on the farther pole side as compared to the closer pole side [Fig. 2(b), middle and bottom]. This difference is the main reason for a larger average antiparallel MT overlap length and consequently a greater number of motor proteins on the farther pole side.

In order to understand how the number of motor proteins changes during chromosome congression, we explore the time course of the average length of antiparallel overlap and the number of kinetochore MTs, as these two quantities directly influence the number of motor proteins [see Eq. (7)]. We find that in the initial kinetochore position, the number of kinetochore MTs on the proximal pole side is almost three times greater, but because of the large difference in the antiparallel overlap lengths on the proximal and farther pole sides, the number of motor proteins is greater on the farther pole side [Fig. 2(c)]. As kinetochores approach the final position they slow down and the number of kinetochore MTs and antiparallel overlaps become equal on both sides.

In our model, motor proteins generate forces that are directed toward the equatorial plane and thus drive chromosome congression. To visualize the centering efficiency, we plot the velocity of kinetochores as a function their position (Fig. 3). We show the effects of both increasing and decreasing, by factor of 2, three relevant parameters: the motor protein velocity without a load, the density of motor proteins, and the MT-kinetochore effective drag coefficient. We observe that the kinetochore velocity is oriented toward the center regardless of its position or changes in parameters. For kinetochores near the poles, the velocity magnitude is close to $v_0/2$, decreasing as they approach the center, where it eventually reaches zero.

Furthermore, we explore kinetochore movement for different values of average MT length. As expected, there is no congression for very short MTs, because there are no kinetochore MTs on the farther pole side [Fig. 4(a), case 1], but congression proceeds normally when the MTs are long

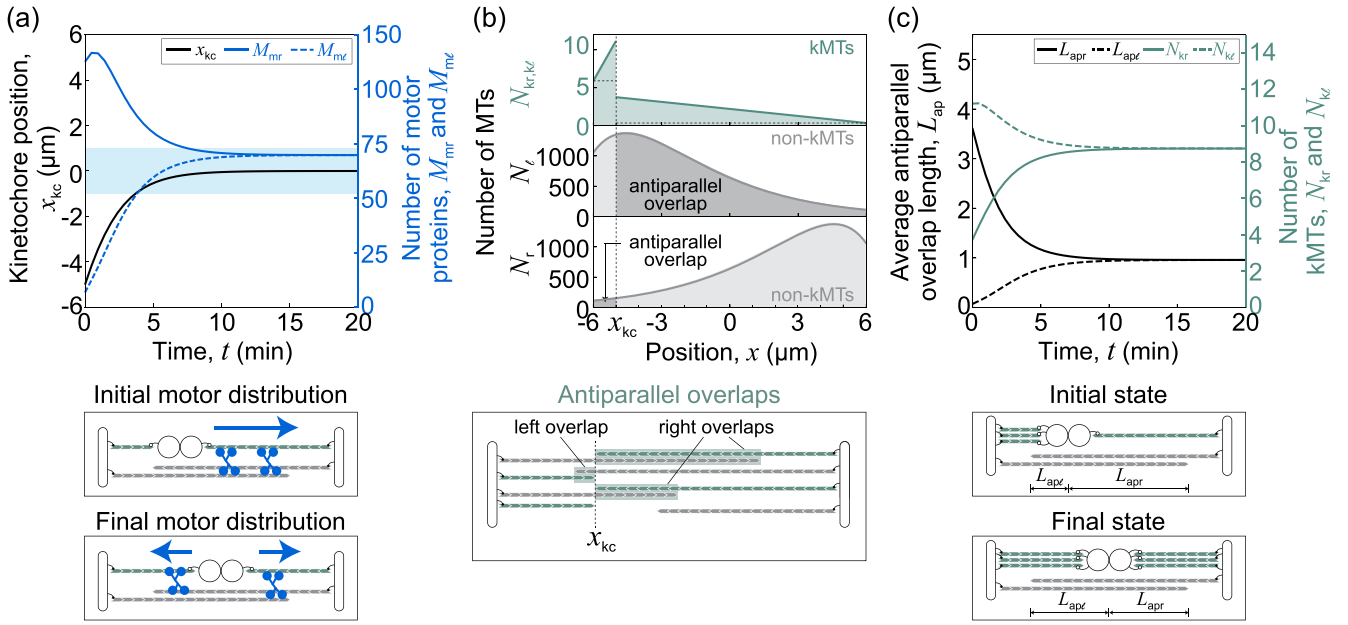

FIG. 2. Motor proteins drive chromosome congression. (a) Solutions of the model for a case with only motor proteins, showing the time course of kinetochore position (black solid line) and the number of motor proteins on the right (blue solid line) and left (blue dashed line) for kinetochores initially at $x = -5$ μm. The blue area indicates the spindle equator zone. Schemes below (a) depict motor proteins (blue pictograms) and forces they exert (arrows) for initial and final kinetochore positions. (b) Distributions of kinetochore MTs (top) and of nonkinetochore MTs (middle and bottom). The shaded regions indicate the fraction of MTs that form antiparallel overlaps with the kinetochore MTs. The number of right kinetochore MTs, at positions to the right of $x_{kc} = -5$ μm, is calculated as $N_{kp} + N_{kn}(x)$, whereas the number of left kinetochore MTs, at positions to the left of x_{kc}, is calculated analogously. Analytical expressions for MT distributions on the left-side $N_{kp\ell}$, $N_{kn\ell}(x)$, and N_ℓ are given in Eqs. (D5), (D7), and (C10), respectively. The scheme below (b) depicts antiparallel overlaps for kinetochores at position x_{kc}. (c) Time course of average antiparallel overlap length (black lines) and number of kinetochore MTs (green lines) for kinetochore positions as in (a). Solid lines represent values for the right side of the model, while dashed lines represent values for the left side. Schemes below (c) depict the number of attached kinetochore MTs and the average antiparallel overlap length for initial and final kinetochore positions. The parameters are given in Tables I and II, except for $c_c = 0$ and $N_{CE} = 0$.

enough to reach the kinetochore from the farther pole side [Fig. 4(a), cases 2 and 3].

By calculating the velocity of the kinetochores as a function of the MT length, we find that for all lengths the velocity is directed toward the center [Fig. 4(b)]. These calculations show that the kinetochore velocity reaches a maximum value for the average MT length around 1 μm. The kinetochore velocity has values comparable to biologically relevant values, which are around 0.5 μm/min [25], for an average MT length between 0.6 and 3.8 μm. To understand how the kinetochore velocity reaches the maximum value, we explore the dependence of the number of motor proteins on the average MT lengths [Fig. 4(c)]. For small average MT lengths, the number of motor proteins is small. By increasing the MT length, the number of motor proteins, and consequently their force, increases, overcoming the chromosome drag friction, resulting in a greater kinetochore velocity [see Eq. (19)]. On the other hand, a further increase in the average MT length results in a smaller ratio between the numbers of motor proteins on both sides, resulting in a decrease in the kinetochore velocity, even though the number of motor proteins still increases.

In order to understand the relationship between the number of motor proteins and the average MT length, we explore changes in MT distributions. These distributions are represented by the length of antiparallel overlaps and the number of MTs attached to each kinetochore, the product of which is proportional to the number of motor proteins [see Eq. (7)]. For small average MT lengths, we find a significant difference in length between left and right overlaps [see Fig. 4(d) for l_0 below 2 μm], which remains for different average MT length, even though both lengths increase. This difference is the main reason for a greater number of motor proteins on the farther pole side. The number of kinetochore MTs is smaller on the farther pole side for smaller average MT lengths, but above 6 μm their difference becomes negligible. The relative difference in the number of kinetochore MTs on both sides is smaller as compared to the relative difference of the antiparallel overlap lengths, and thus the number of motor proteins is greater on the farther pole side.

B. Forces exerted by passive cross-linkers impair chromosome congression

In the preceding section, we showed that motor proteins distributed along antiparallel regions drive chromosome congression. Here we explore to what extent passive cross-linkers accumulating in parallel regions affect chromosome congression. Unlike motor proteins, passive cross-linkers cannot generate active forces by themselves, and for this reason one can assume that passive cross-linkers cannot have an active role in chromosome congression. However, this reasoning changes when passive cross-linkers act in combination with

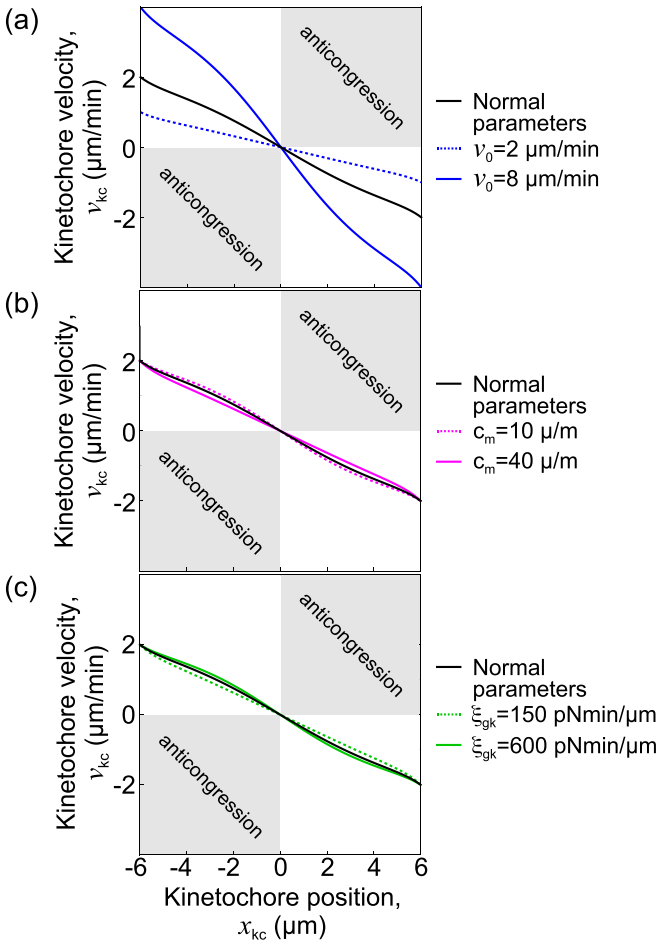

FIG. 3. Kinetochore velocities as a function of the kinetochore position for the original parameters as well as two times greater and lower motor (a) protein velocity without a load, (b) density of motor proteins, and (c) MT-kinetochore effective drag coefficient. The changed parameters are given in the legend. The remaining parameters are given in Tables I and II, except for $c_c = 0$ and $N_{CE} = 0$.

active processes that generate directed movement. In our case, the directed movement of bridging MTs, poleward flux, drives the movement of kinetochore MTs as they are connected by passive cross-linkers. Thus, we explore the positioning of the kinetochores in our system in the presence of passive cross-linkers, but without motor proteins on the kinetochore MTs.

To study the role of cross-linkers in chromosome congression, we analyze the kinetochore velocity in the limit where the numbers of motor proteins and kinetochore motor proteins go to zero ($M_{mr,m\ell} = 0$ and $N_{CE} = 0$), for which Eq. (18) simplifies to

$$v_{kc} = \frac{v_0}{2}\frac{\frac{M_{cr}}{M_{c\ell}} - 1}{\frac{M_{cr}}{M_{c\ell}} + 1}\left[1 + \frac{\eta}{\xi_c} + \frac{\eta\xi_{gk}}{\xi_c^2(M_{cr} + M_{c\ell})} + \left(2\frac{\xi_c}{\xi_{gk}} + \frac{\eta}{\xi_{gk}}\right)\frac{M_{cr}M_{c\ell}}{M_{cr} + M_{c\ell}}\right]^{-1} \quad (20)$$

This equation shows that kinetochores move toward the side with a greater number of passive cross-linkers, which is similar to kinetochore movement driven by motor proteins [see Eq. (19)]. Because passive cross-linkers accumulate in parallel overlaps and motor proteins in antiparallel overlaps, we expect their distributions to differ and thus differently affect chromosome congression.

Our numerical calculations show that for biologically relevant MT lengths, the kinetochores do not approach the spindle center. Instead, they asymptotically approach one of two stable points located near poles, with the point the kinetochores approach depending on their initial position [Fig. 5(a)].

To further explore the kinetochore movement, we show the dependence of kinetochore velocity on its position for different values of the average MT length [Fig. 5(b)]. For average MT lengths $l_0 = 1.3$ and 2.6 μm there are two stable points placed symmetrically with respect to the unstable point located in the center. We refer to these three points as fixed points. For larger average MT lengths $l_0 = 6$ μm, the central location changes stability and becomes a unique stable fixed point that the kinetochores approach irrespective of its initial position.

To describe the system in the vicinity of the central fixed point, we explore the stability of this point [Fig. 5(c)]. By numerically calculating Eq. (E1), we find that the system undergoes a supercritical pitchfork bifurcation with a critical average MT length of $l^* \approx 3$ μm. In this case, above the critical MT length there is only one stable fixed point in the center. Below the critical MT length the central fixed point becomes unstable, and the transition in stability is accompanied by the appearance of two stable fixed points.

To gain an intuitive explanation why the fixed point in the center changes its stability, we depict distributions of MTs for three different average MT lengths [Fig. 5(d)]. For small average MT lengths, MTs do not reach kinetochores from the far pole side, whereas from the near pole side, MTs reach the kinetochore (case 1). In this case passive cross-linkers accumulate within the parallel overlap at the near pole side only and thus generate off-centering force. As the average MT length increases, MTs reach the kinetochore from the far pole side and cross-linkers accumulate at both sides, resulting in similar forces on both kinetochores (case 2). For large average MT lengths, the number of kinetochore MTs becomes similar on both sides, thus a longer overlap on the farther pole side accumulates more cross-linkers, producing a centering force (case 3).

C. Collective forces of motor proteins and cross-linkers determine the direction of chromosome movement

In previous sections, we separately explored the influence of motor proteins and cross-linkers on chromosome congression, whereas in real biological systems they work together, and thus we explore their combined contribution. For biologically relevant parameters, the kinetochores that were initially displaced from the spindle center approach it in several minutes [Fig. 6(a)]. This outcome occurs regardless of initial conditions, for kinetochores close to the pole and those closer to the center. The dynamics of this process are similar to those in the case without cross-linkers [Fig. 2(a)], implying that motor proteins generate dominant forces during chromosome congression.

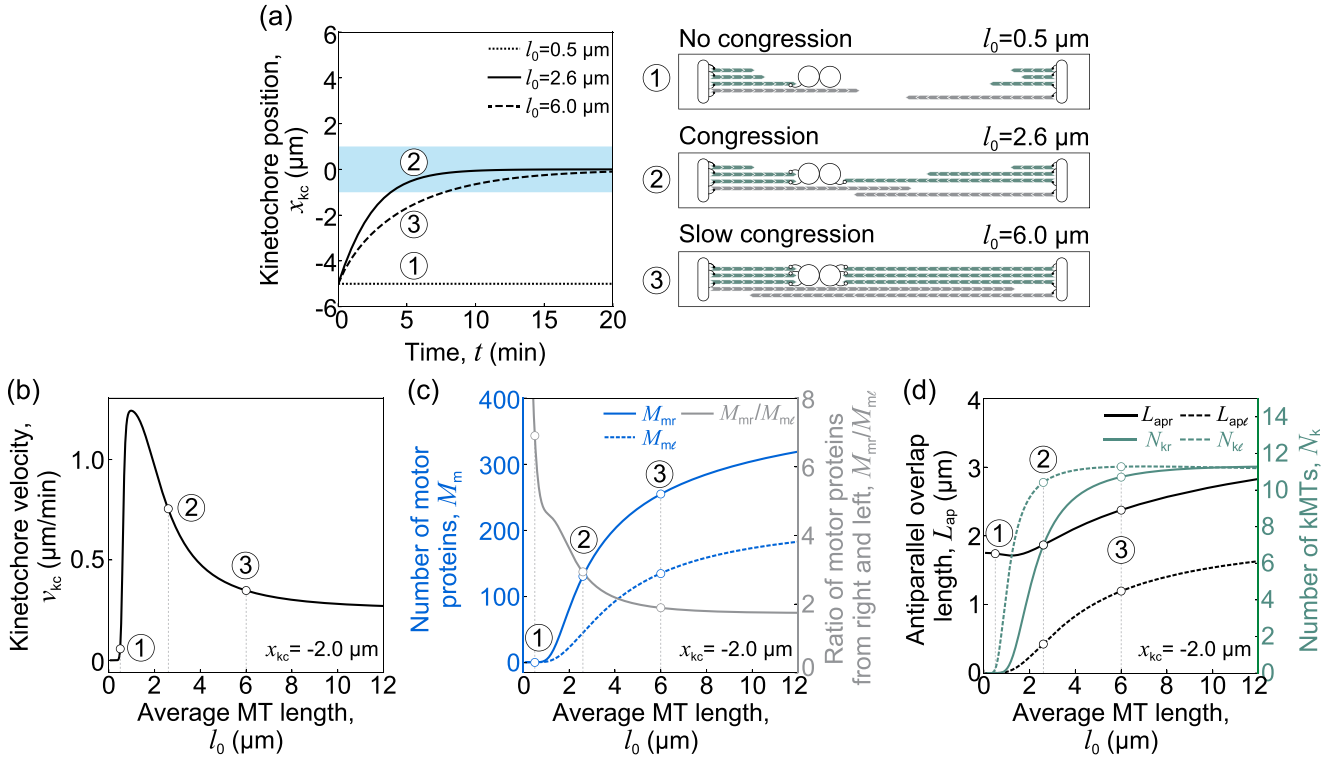

FIG. 4. Congression velocity depends on average MT length. (a) Shown on the left are solutions of the model showing the time course of the kinetochore position for kinetochores initially at $x_{kc} = -5$ μm for different average MT lengths: Cases with small MT length $l_0 = 0.5$ μm (dotted line), normal MT length $l_0 = 2.6$ μm (solid line), and large MT length $l_0 = 6$ μm (dashed line) are denoted by encircled numbers 1–3, respectively. The light blue area indicates the spindle equator zone. Shown on the right are schematic representations of the dependence of the numbers of kinetochore MTs corresponding to case 1, with no kinetochore MTs on the right kinetochore; case 2, with few kinetochore MTs on the right kinetochore; and case 3, with the same number of kinetochore MTs on both kinetochores. (b) Dependence of kinetochore velocities on average MT lengths. (c) Number of motor proteins on the right (blue solid line) and left sides (blue dashed line) and their ratio (gray line) as a function of the average MT length. (d) Average antiparallel overlap length of the right (black solid line) and left (black dashed line) kinetochore MTs and the number of kinetochore MTs (right y axis) on the right (green solid line) and left (green dashed line) kinetochore as a function of the average MT length. In (b)–(d) kinetochores are at position $x_{kc} = -2$ μm. The encircled numbers 1–3 show the values corresponding to the average MT lengths as in cases from (a). The remaining parameters are given in Tables I and II, except for $c_c = 0$ and $N_{CE} = 0$.

Our results show that the average MT length plays an important role in chromosome movement. To explore how the velocity of kinetochores depends on their position when both motor proteins and cross-linkers are present, we plot this dependence for two different values of average MT lengths [Fig. 6(b)]. For parameters as in Tables I and II, all velocities are directed toward the stable central position. However, for smaller average MT lengths, there are three stable fixed points and two unstable fixed points located between neighboring stable fixed points, leading to increased complexity in the kinetochore movement.

Next we explore the stability of the central position for different values of cross-linker density [Fig. 6(c)]. For a wide range of cross-linker densities, the central position is the only fixed point and all kinetochores move toward it, irrespective of the starting position. When the concentration exceeds a critical value, the central location becomes unstable and two new stable fixed points appear symmetrically with respect to the center, which is a signature of supercritical pitchfork bifurcation. Further, we explore the parameter space by studying kinetochore movement in the vicinity of the central fixed point, as in Appendix E. We find that the critical cross-linker density, for which the central fixed point changes its stability, is linearly proportional to the density of motor proteins [Fig. 6(d)]. For values below the critical cross-linker density, congression proceeds normally, while for values above it chromosomes move away from the center.

Motivated by the complex kinetochore dynamics for smaller average MT lengths [Fig. 6(b)], we explore the transitions that occur in this region of parameter space. Using cross-linker density as a control parameter, we plot the position of stable and unstable fixed points [Fig. 6(e)]. The results show a subcritical pitchfork bifurcation, where an unstable fixed point becomes stable, and two new unstable fixed points emerge as the cross-linker density decreases. For the same cross-linker densities there are two stable fixed points and they coexist with the unstable fixed points, on both sides of the bifurcation.

Depending on the number of stable fixed points, we identify three distinct regions in the parameter space [Fig. 6(f)]. These results suggest that, when there is more than one stable fixed point, congression fails and kinetochores can be stably located both near the poles and at the center.

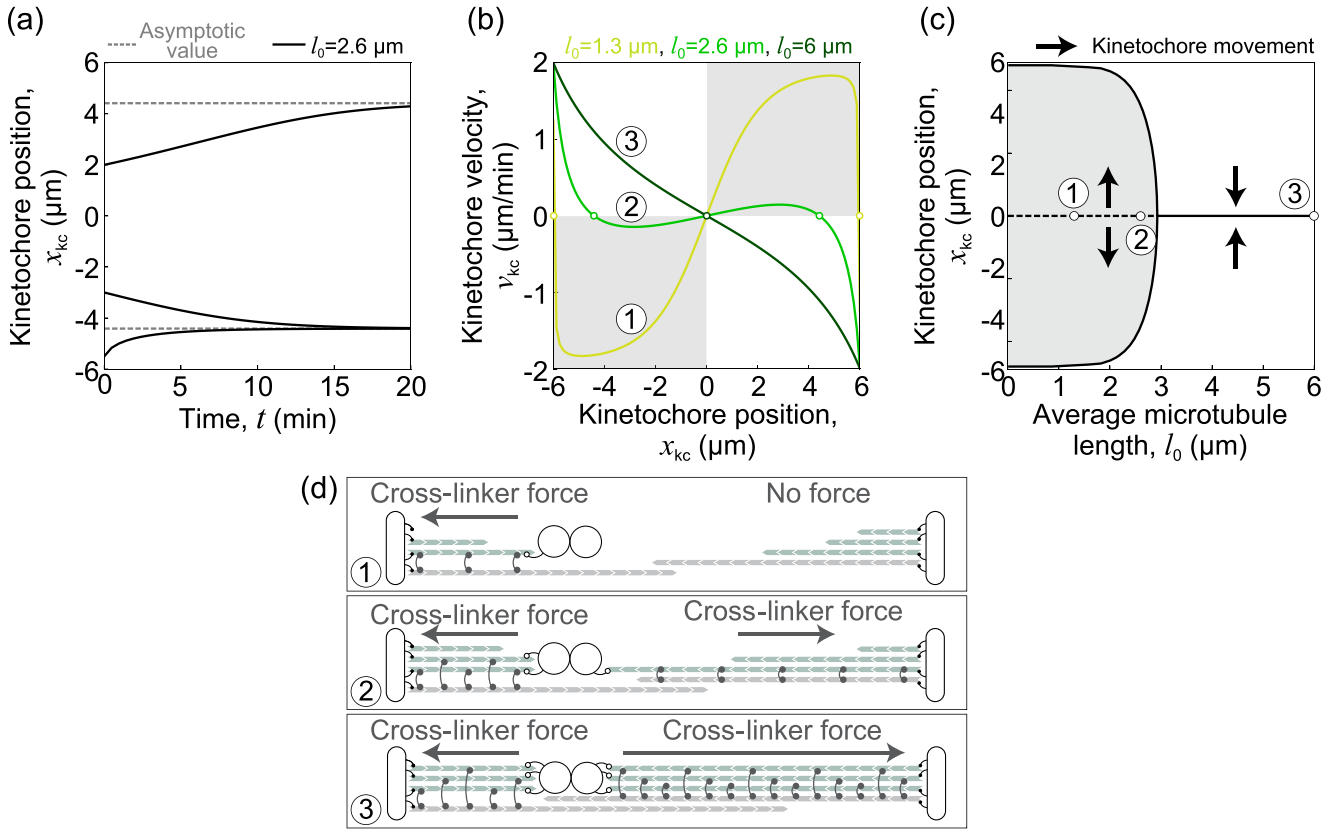

FIG. 5. Passive cross-linkers produce forces that can oppose chromosome congression. (a) Time courses of the kinetochore positions (black lines) driven by cross-linkers for the kinetochore starting at three different positions $x_{kc} = -5$, -3, and 2 μm. The kinetochores approach one of two asymptotic positions (gray dashed lines). (b) Dependence of the kinetochore velocity on the kinetochore position along the MT spindle for three different average MT lengths: short MTs $l_0 = 1.3$ μm (case 1, pear green line), normal MT lengths $l_0 = 2.6$ μm (case 2, green line), and long MTs $l_0 = 6$ μm (case 3, dark green line). The gray areas represent the choice of positions and velocities for which the kinetochores will move toward the closer pole. White dots represent stable fixed points for different average MT lengths. (c) Positions of the stable (black solid line) and unstable (black dashed line) fixed points for different average MT lengths. The gray area represents the choice of positions and MT lengths for which the kinetochores will move toward the closer pole. The kinetochore movement direction is indicated by the black arrows. (d) Schematic depiction of forces exerted by cross-linkers (black) on kinetochores (white) for short MTs (case 1), intermediate MTs (case 2), and long MTs (case 3). The force magnitude and direction of each kinetochore are indicated by an arrow. In (a)–(c) the unchanged parameters are given in Tables I and II, except for $c_m = 0$ and $N_{CE} = 0$.

D. Plus-end-directed kinetochore motor proteins assist chromosome congression

In addition to motor proteins and cross-linkers, our model also describes kinetochore motor proteins that contribute to chromosome congression by transporting chromosomes along MTs toward their plus ends. In order to isolate the influence of kinetochore motor proteins on chromosome congression, we set the number of motor proteins and cross-linkers in Eq. (18) to zero, yielding the kinetochore velocity

$$v_{kc} = \left(v_{CE0} - \frac{v_0}{2}\right)\frac{\frac{N_\ell}{N_r} - 1}{\frac{N_\ell}{N_r} + 1}\left(1 + \frac{\eta v_{CE0}}{2N_{CE} f_{CE0}}\right)^{-1}. \qquad (21)$$

Here we see that the kinetochore velocity direction depends on the difference between the kinetochore-motor-protein velocity without a load and the nonkinetochore-MT flux velocity. This suggests that kinetochore-motor-protein-driven chromosome congression is possible when these motors are faster than the poleward flux, providing an explanation for different directions of chromosome movement in Fig. 7(a). Based on Eq. (21), we also find that the kinetochore velocity depends on the ratio of the number of left and right nonkinetochore MTs, whereas calculations in Appendix F show under which conditions kinetochore motor proteins generate anticongression.

To explore how kinetochore motor proteins work together with motor proteins and cross-linkers to promote congression, we plot a phase diagram by varying the cross-linker and motor protein densities [Fig. 7(b)]. These calculations reveal that chromosome congress in a large fraction of parameter space. In comparison with Fig. 6(d), we observe that the region of parameter space for which chromosomes congress increases in the presence of kinetochore motor proteins, suggesting that they promote chromosome congression. Taken together, our theory shows that length-dependent poleward flux drives chromosome congression for a broad range of biologically relevant parameters.

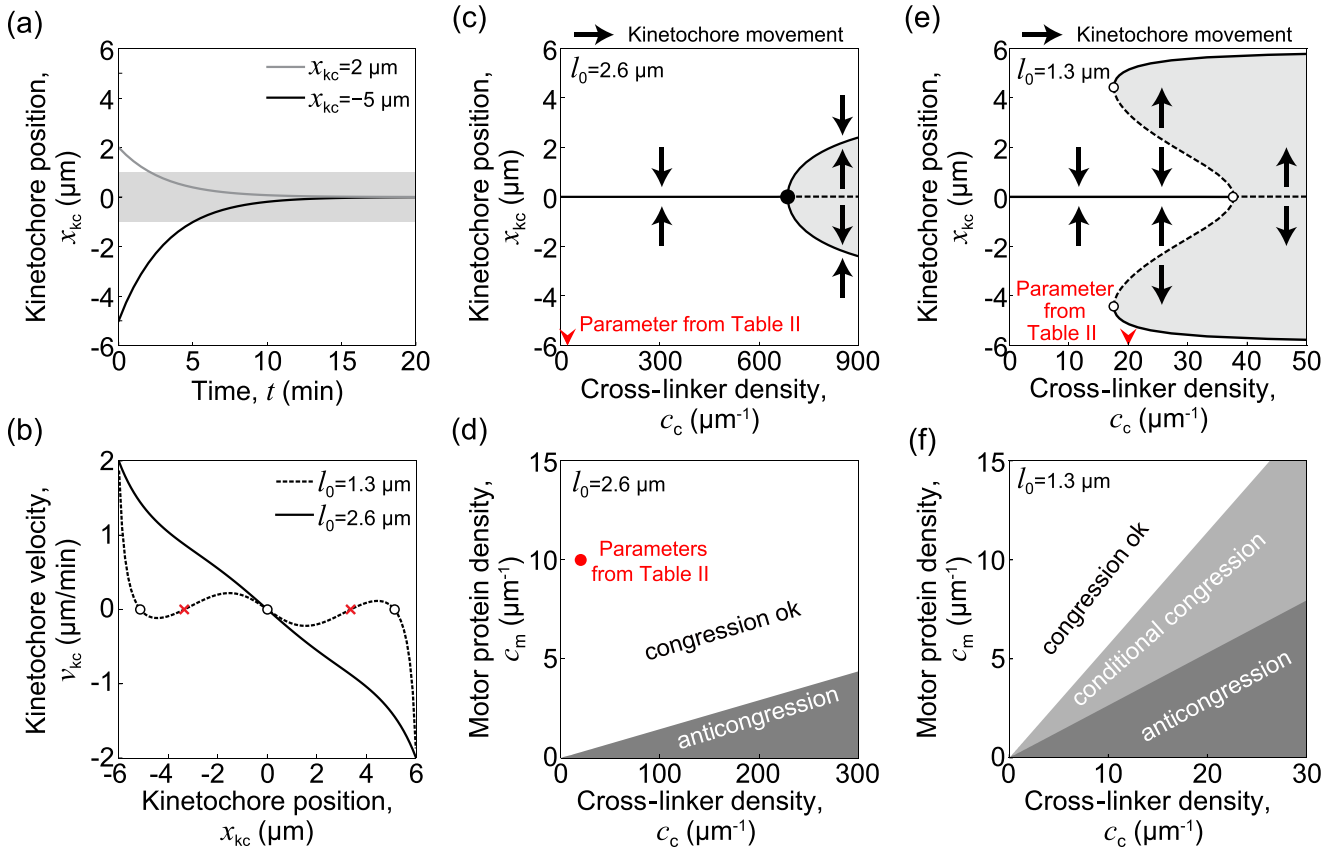

FIG. 6. Interplay of motor protein and cross-linker forces regulates the effectiveness of chromosome congression. (a) Solutions of the model showing the time course of the kinetochore position for kinetochores initially at $x = 2$ μm (gray line) and $x = -5$ μm (black line). The blue area indicates the spindle equator zone. (b) Dependence of the kinetochore velocity on the kinetochore position for two different MT lengths $l_0 = 3$ μm (black line) and $l_0 = 1.5$ μm (gray line). The dots represent the stable fixed points, whereas the red crosses denote the unstable fixed points. (c) Position of the stable (black solid line) and unstable (black dashed line) points for different average cross-linker densities and MT length $l_0 = 2.6$ μm. The arrow on the x axis represents the cross-linker density c_c given in Table II. The kinetochore movement direction is indicated by the black arrows. (d) Phase diagram showing a region where congression occurs for different cross-linker and motor protein densities for MT length $l_0 = 2.6$ μm. The transition line occurs at $c_m \approx 0.019 c_c$. The red dot represents the density values given in Table II. (e) Position of the stable (black solid line) and unstable points (black dashed line) for different average cross-linker densities and MT length $l_0 = 1.3$ μm. (f) Phase diagram showing a region where congression occurs for different cross-linker and motor protein densities and MT length $l_0 = 1.3$ μm. The two transition lines occur at $c_m \approx 0.67 c_c$ and $0.29 c_c$. The kinetochore movement direction is indicated by the black arrows. The remaining parameters are given in Tables I and II, except for $N_{CE} = 0$.

IV. DISCUSSION

Our model highlights the importance of forces proportional to MT overlap lengths in chromosome congression. Our calculations show that motor proteins, which accumulate in antiparallel overlaps, at long kinetochore MTs produce forces that overcome those generated on the shorter kinetochore MTs, resulting in chromosome congression. Conversely, passive cross-linkers produce forces that pull the chromosomes toward the closer pole, opposing congression. Crucially, the forces generated by the motor proteins are large enough to overcome the forces that oppose congression. Our calculations also show that plus-end-directed motor proteins at kinetochores assist congression. Thus, our model provides a suitable tool for studying forces relevant for chromosome congression and reproduces experimentally measured kinetochore velocities, including the duration of chromosome congression.

It has been shown that regulation of the length of MTs attached to kinetochores is essential for optimal congression velocity, where the MT dynamics is controlled by motor protein Kif18A, which accumulates in a length-dependent manner [30,75,76]. Our model provides an alternative explanation, where kinetochore MTs form overlaps with nonkinetochore MTs and thus exert forces that are length dependent (Fig. 2). These two mechanisms do not oppose each other, and thus they can work together, but future experiments will clarify the contribution of each individual mechanism.

In experiments in cells with altered concentrations of CENP-E proteins, chromosomes can be found in the metaphase plane, as well as near the poles [25]. Such states can persist for long periods of time, even after inhibiting Aurora B (which detaches kinetochore MTs at low interkinetochore tension), suggesting that there are several stable locations along the spindle where kinetochores tend to accumulate. Our model predicts that a regime with multiple stable

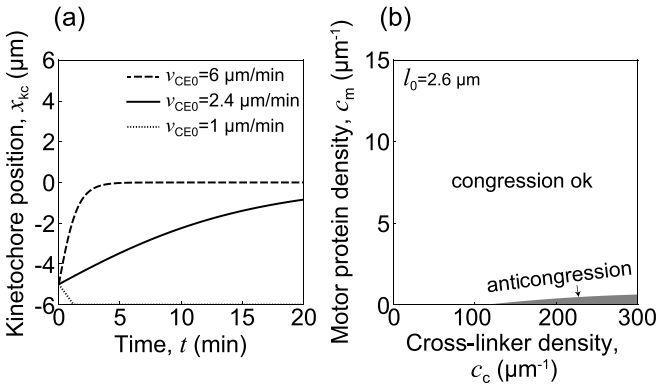

FIG. 7. Chromosome congression with kinetochore motor proteins alone and in combination with other proteins. (a) Solutions of the model showing the time course of the kinetochore position driven by kinetochore motor proteins affecting the kinetochore MTs starting at $x_{kc} = -5$ μm for different velocities without a load of the kinetochore motor proteins. (b) Phase diagram showing a region where congression occurs for different cross-linker and motor protein densities. The remaining parameters are given in Tables I and II.

points can appear. For example, in spindles with small average MT length, stable points in the center and near the pole coexist, and kinetochores approach one of them, depending on the initial position [Figs. 6(b), 6(e), and 6(f)]. A close comparison of our theoretical predictions and experiments that quantify the distribution of MTs attached to kinetochores will provide deeper insight into the mechanisms that help in the correction of these erroneous states.

Our model describes the movement of one chromosome, implying that chromosomes move independent of each other. The study of chromosome movement during the metaphase shows that chromosomes typically move independently of each other, but in the case of neighboring chromosomes there is a certain correlation in the movement of chromosomes [77]. Based on this observation, it was proposed that the correlation is a consequence of the interaction between kinetochore MTs of neighboring chromosomes. In our mechanism of chromosome congression, forces at kinetochore MTs arise from interactions with neighboring MTs. Thus, extending the model to include multiple chromosomes and the interaction between their kinetochore MTs could result in correlated movement of neighboring chromosomes. Future studies, theoretical and experimental, will reveal to what extent chromosome movement is correlated during congression.

During mitosis, MTs from one side can attach to either kinetochore and occasionally form erroneous, merotelic or syntelic attachments [78,79]. These types of errors are typical in tumor cells, so it would be interesting to explore the formation and correction of such attachments by a theoretical model. Our model could be generalized by describing MT attachment to kinetochores from both sides, as well as the observed tension-dependent MT detachment from kinetochores [62,80] and Aurora B activity [81–83]. Such a model could provide a deeper understanding of the correction of different types of erroneous attachments.

Our model describes chromosome congression, but the framework we propose can also be extended to metaphase. For instance, it may offer insights into the centering forces that govern kinetochore oscillations. In existing models, the centering force is typically attributed to polar ejection force [53,55,56]. Future studies will help determine which centering force plays the dominant role in driving kinetochore oscillations.

In conclusion, we introduced a model that describes the most important forces that appear during chromosome congression, and therefore it represents a powerful tool for studying this biological process. This model relies on length-dependent poleward flux and describes MT distributions in mean-field approximation, which allows us to systematically explore the parameter space and distinguish the contributions of different mechanisms.

ACKNOWLEDGMENTS

We thank Kruno Vukušić, Iva Tolić, and Patrick Meraldi for valuable discussions and help in comparing experiments and theory, Maja Novak and Shane Amadeus Fiorenza for comments on the manuscript, and other members of the NP and IMT research groups for their feedback. This work was funded by the European Research Council through ERC Synergy Grant No. 855158 (granted to N.P.) and cofunded by the Croatian Science Foundation through Project No. IP-2019-04-5967 (granted to N.P.)

APPENDIX A: EQUATIONS OF MOVEMENT OF THE LEFT AND RIGHT KINETOCHORES

In the main text we focused on equations describing the movement of the center of mass of sister kinetochores. Here we present the full equations describing the movements of the left and right kinetochore and how to get the center-of-mass equations. The equations of movement of the left and right kinetochores are given as

$$\frac{\eta}{2} v_{\mathrm{kc}\ell} = F_{\mathrm{kMT}\ell} + F_{\mathrm{CE}\ell} + F_{\mathrm{KI}}, \tag{A1}$$

$$\frac{\eta}{2} v_{\mathrm{kcr}} = F_{\mathrm{kMTr}} + F_{\mathrm{CEr}} - F_{\mathrm{KI}}, \tag{A2}$$

where $v_{\mathrm{kc}\ell} \equiv \frac{\mathrm{d}x_{\mathrm{kc}\ell}}{\mathrm{d}t}$ and $v_{\mathrm{kcr}} \equiv \frac{\mathrm{d}x_{\mathrm{kcr}}}{\mathrm{d}t}$ denote the velocities of the left and right kinetochores, respectively, and F_{KI} denotes the force of interaction between two kinetochores. Inserting these two equations into the definition of the position of the center of mass of sister kinetochores $x_{\mathrm{kc}} = \frac{x_{\mathrm{kc}\ell} + x_{\mathrm{kcr}}}{2}$, we get Eq. (1), rewritten as

$$\eta \frac{\mathrm{d}x_{\mathrm{kc}}}{\mathrm{d}t} = F_{\mathrm{kMTr}} + F_{\mathrm{kMT}\ell} + F_{\mathrm{CEr}} + F_{\mathrm{CE}\ell}. \tag{A3}$$

In the paper we approximate each of these forces as a function of the position of the center of mass of the left and right kinetochores only and not the positions of the individual kinetochores. In order to be able to calculate the velocity of the kinetochores it is necessary to provide further definitions for the left- and right-side functions. Kinetochore MT growth velocities, defined as

$$v_{\mathrm{gkr},\ell} \equiv \pm(v_{\mathrm{kfr},\ell} - v_{\mathrm{kc}}), \tag{A4}$$

are calculated as

$$v_{\mathrm{gkr},\ell} = \frac{\pm 1}{\xi_{\mathrm{gk}}}(M_{\mathrm{mr},\ell} f_{\mathrm{mr},\ell} + M_{\mathrm{cr},\ell} f_{\mathrm{cr},\ell}). \tag{A5}$$

Here and in the following Appendixes the upper sign (+ or −) corresponds to the right-side index r and the lower sign corresponds to the left-side index ℓ. The average force per motor protein $f_{\mathrm{mr},\ell}$ for both sides is calculated as

$$f_{\mathrm{mr},\ell} = f_0\left(\pm 1 - \frac{v_{\mathrm{kfr},\ell} - v_{\mathrm{f}\ell,\mathrm{r}}}{v_0}\right). \tag{A6}$$

Similarly, the average drag force per cross-linker is calculated as

$$f_{\mathrm{cr},\ell} = -\xi_{\mathrm{c}}(v_{\mathrm{kfr},\ell} - v_{\mathrm{fr},\ell}). \tag{A7}$$

Additionally, the forces due to kinetochore motor proteins stepping toward the right or left are calculated as

$$f_{\mathrm{CEr},\ell} = f_{\mathrm{CE0}}\left(\pm 1 - \frac{v_{\mathrm{kc}} - v_{\mathrm{f}\ell,\mathrm{r}}}{v_{\mathrm{CE0}}}\right), \tag{A8}$$

where we redefine the average kinetochore-motor-protein force, as $f_{\mathrm{CE,pp}\ell} = f_{\mathrm{CE,apr}} = f_{\mathrm{CEr}}$ and $f_{\mathrm{CE,ppr}} = f_{\mathrm{CE,ap}\ell} = f_{\mathrm{CE}\ell}$. The equations governing nonkinetochore-MT distributions for the left and right sides are identical to those in Eqs. (9)–(12) by form. However, in Eq. (11) the number of pole MTs at position x pointing toward the left, $N_{\mathrm{pr}}(x)$, is connected to the number of pole MTs at position x pointing toward the right as $N_{\mathrm{p}\ell}(x) = N_{\mathrm{pr}}(-x)$. The equations for the distributions of kinetochore MTs on the left and right kinetochores differ in one term due to the kinetochore velocity affecting the attachment:

$$\frac{\mathrm{d}N_{\mathrm{kpr},\ell}}{\mathrm{d}t} = (v_{\mathrm{g}} \pm v_{\mathrm{kc}}) p_{\mathrm{att}}\left(1 - \frac{N_{\mathrm{kr},\ell}}{N_0}\right) n_{\mathrm{p}}|_{l=L/2\mp x_{\mathrm{kc}}} - k_{\mathrm{off}} N_{\mathrm{kpr},\ell}, \tag{A9}$$

$$\frac{\partial n_{\mathrm{knr},\ell}}{\partial t} = (v_{\mathrm{g}} \pm v_{\mathrm{kc}}) p_{\mathrm{att}}\left(1 - \frac{N_{\mathrm{kr},\ell}}{N_0}\right) \rho_{\mathrm{nr},\ell}|_{x=x_{\mathrm{kc}}\pm l} - k_{\mathrm{off}} n_{\mathrm{knr},\ell}. \tag{A10}$$

The number of kinetochore MTs on the right and left kinetochores is calculated as

$$N_{\mathrm{kr},\ell} = N_{\mathrm{kpr},\ell} + \int_0^{L/2\mp x_{\mathrm{kc}}} n_{\mathrm{knr},\ell}\, dl \tag{A11}$$

and the average parallel and antiparallel overlap lengths are calculated as

$$L_{\mathrm{apr,ppr}} = \frac{1}{N_{\mathrm{kr}}}\left(N_{\mathrm{kpr}} \int_{x_{\mathrm{kc}}}^{L/2} dx\, P_{\ell,\mathrm{r}} + \int_0^{L/2-x_{\mathrm{kc}}} dl\, n_{\mathrm{kn}} \int_{x_{\mathrm{kc}}}^{x_{\mathrm{kc}}+l} dx\, P_{\ell,\mathrm{r}}\right), \tag{A12}$$

$$L_{\mathrm{ap}\ell,\mathrm{pp}\ell} = \frac{1}{N_{\mathrm{k}\ell}}\left(N_{\mathrm{kp}\ell} \int_{x_{\mathrm{kc}}}^{L/2} dx\, P_{\mathrm{r},\ell} + \int_0^{L/2+x_{\mathrm{kc}}} dl\, n_{\mathrm{kn}} \int_{x_{\mathrm{kc}}-l}^{x_{\mathrm{kc}}} dx\, P_{\mathrm{r},\ell}\right). \tag{A13}$$

Here we presented the equations for the left and right sides corresponding to Eqs. (1)–(17).

APPENDIX B: CALCULATING THE KINETOCHORE VELOCITY

In order to calculate the kinetochore velocity v_{kc}, we start with the equations for the balance of forces on the kinetochore,

$$\eta v_{\mathrm{kc}} = F_\ell + F_{\mathrm{r}}, \tag{B1}$$

and by applying Eqs. (6) and (8) we get

$$\eta v_{\mathrm{kc}} = M_{\mathrm{mr}} f_{\mathrm{mr}} + M_{\mathrm{m}\ell} f_{\mathrm{m}\ell} + M_{\mathrm{cr}} f_{\mathrm{cr}} + M_{\mathrm{c}\ell} f_{\mathrm{c}\ell} + 2N_{\mathrm{CE}}(f_{\mathrm{CEr}} P_{\mathrm{r}} + f_{\mathrm{CE}\ell} P_\ell), \tag{B2}$$

where we applied the redefinition of the kinetochore-motor-protein forces as in Eq. (A8). We proceed by inserting the force-velocity expression from Eqs. (A6)–(A8). The sum of the kinetochore-associated motor protein forces is

$$2N_{\mathrm{CE}}(f_{\mathrm{CEr}} P_{\mathrm{r}} + f_{\mathrm{CE}\ell} P_\ell) = 2N_{\mathrm{CE}} f_{\mathrm{CE0}} \frac{v_{\mathrm{CE0}} - v_0/2}{v_{\mathrm{CE0}}}(P_\ell - P_{\mathrm{r}}) - 2N_{\mathrm{CE}} \frac{f_{\mathrm{CE0}}}{v_{\mathrm{CE0}}} v_{\mathrm{kc}}, \tag{B3}$$

where we used $v_{\mathrm{fr},\ell} = \pm v_0/2$ and $P_\ell + P_{\mathrm{r}} = 1$. The sum of the forces due to motor proteins and cross-linkers on the kinetochore MTs follows as

$$M_{\mathrm{mr}} f_{\mathrm{mr}} + M_{\mathrm{m}\ell} f_{\mathrm{m}\ell} + M_{\mathrm{cr}} f_{\mathrm{cr}} + M_{\mathrm{c}\ell} f_{\mathrm{c}\ell} = \beta_{\mathrm{r}}\left(\frac{v_0}{2} - v_{\mathrm{kfr}}\right) + \beta_\ell\left(-\frac{v_0}{2} - v_{\mathrm{kfl}}\right), \tag{B4}$$

where we used a shorthand notation $\beta_{\mathrm{r},\ell} = M_{\mathrm{mr},\ell}\frac{f_0}{v_0} + M_{\mathrm{cr},\ell}\xi_{\mathrm{c}}$. To find the kinetochore-MT flux velocities $v_{\mathrm{kfr},\ell}$, we use the equations for the growth of kinetochore MTs [Eq. (A5)] and by inserting the force-velocity expression from Eqs. (A6)–(A8) we get

$$v_{\mathrm{kfr}} = \frac{\xi_{\mathrm{gk}}}{\xi_{\mathrm{gk}} + \beta_{\mathrm{r}}} v_{\mathrm{kc}} + \frac{\beta_{\mathrm{r}}}{\xi_{\mathrm{gk}} + \beta_{\mathrm{r}}}\frac{v_0}{2}, \tag{B5}$$

$$v_{\mathrm{kf}\ell} = \frac{\xi_{\mathrm{gk}}}{\xi_{\mathrm{gk}} + \beta_\ell} v_{\mathrm{kc}} - \frac{\beta_\ell}{\xi_{\mathrm{gk}} + \beta_\ell}\frac{v_0}{2}. \tag{B6}$$

Inserting these equations into Eq. (B4) yields an equation that shows the kinetochore velocity as a function of the total number of motor proteins, cross-linkers, and kinetochore-associated motor proteins,

$$v_{\mathrm{kc}} = \frac{v_0}{2}\frac{1}{\gamma_{\mathrm{MT}}}\left(\frac{f_0}{v_0}(M_{\mathrm{mr}} - M_{\mathrm{m}\ell}) + \xi_{\mathrm{c}}(M_{\mathrm{cr}} - M_{\mathrm{c}\ell})\right) + \left(v_{\mathrm{CE0}} - \frac{v_0}{2}\right)\frac{1}{\gamma_{\mathrm{CE}}}\frac{f_{\mathrm{CE0}}}{v_{\mathrm{CE0}}}(N_{\mathrm{CE}} P_\ell - N_{\mathrm{CE}} P_{\mathrm{r}}), \tag{B7}$$

where we introduced the additional shorthand notation $\gamma_{\mathrm{MT}} = (\eta + 2N_{\mathrm{CE}}\frac{f_{\mathrm{CE0}}}{v_{\mathrm{CE0}}})(1 + \frac{\beta_{\mathrm{r}}}{\xi_{\mathrm{gk}}})(1 + \frac{\beta_\ell}{\xi_{\mathrm{gk}}}) + 2\frac{\beta_\ell\beta_{\mathrm{r}}}{\xi_{\mathrm{gk}}} + \beta_{\mathrm{r}} + \beta_\ell$ and $\gamma_{\mathrm{CE}} = \gamma_{\mathrm{MT}}/(1 + \frac{\beta_{\mathrm{r}}}{\xi_{\mathrm{gk}}})(1 + \frac{\beta_\ell}{\xi_{\mathrm{gk}}})$.

APPENDIX C: CALCULATING THE NONKINETOCHORE MICROTUBULE DISTRIBUTIONS

Here we calculate the nonkinetochore-MT distributions in a steady-state limit. The stationary equations for distributions

of nonkinetochore MTs that point rightward, calculated from Eqs. (9)–(12), are given as

$$0 = k_{\mathrm{p}}\delta(l) - k_{\mathrm{ps}}n_{\mathrm{p}\ell} - \frac{\partial v_{\mathrm{g}}n_{\mathrm{p}\ell}}{\partial l}, \tag{C1}$$

$$0 = k_{\mathrm{ps}}n_{\mathrm{p}\ell} - k_{\mathrm{cat}}\tilde{n}_{\mathrm{p}\ell}, \tag{C2}$$

$$0 = k_{\mathrm{n}}c\delta(l)N_{\mathrm{p}}(x) - k_{\mathrm{ps}}\rho_{\mathrm{n}\ell} - \frac{\partial v_{\mathrm{g}}\rho_{\mathrm{n}\ell}}{\partial l}, \tag{C3}$$

$$0 = k_{\mathrm{ps}}\rho_{\mathrm{n}\ell} - k_{\mathrm{cat}}\tilde{\rho}_{\mathrm{n}\ell}. \tag{C4}$$

We solve Eqs. (C1) and (C3) in two steps. First, we find the solutions of the homogeneous part, which for these two equations have the same form with different integration constants $A_{\mathrm{n},\rho}\exp(-\frac{l}{l_0})$, where

$$l_0 \equiv \frac{v_{\mathrm{g}}}{k_{\mathrm{ps}}}. \tag{C5}$$

By taking into account the inhomogeneous terms we calculate the integration constants yielding the stationary distributions of nonkinetochore MTs extending from the pole and those nucleated along preexisting MTs:

$$n_{\mathrm{p}\ell} = \frac{k_{\mathrm{p}}}{v_{\mathrm{g}}}\exp\left(-\frac{1}{l_0}l\right), \tag{C6}$$

$$\rho_{\mathrm{n}\ell} = \frac{k_{\mathrm{n}}c}{v_{\mathrm{g}}}\exp\left(-\frac{1}{l_0}\frac{L}{2}\right)\left(\frac{k_{\mathrm{p}}}{k_{\mathrm{ps}}}+\frac{k_{\mathrm{p}}}{k_{\mathrm{cat}}}\right)\exp\left(-\frac{1}{l_0}(l+x)\right). \tag{C7}$$

The solutions of Eqs. (C2) and (C4) provide a simple relationship between the numbers of growing and pausing MTs:

$$\tilde{n}_{\mathrm{p}\ell} = \frac{k_{\mathrm{ps}}}{k_{\mathrm{cat}}}n_{\mathrm{p}\ell}, \tag{C8}$$

$$\tilde{\rho}_{\mathrm{n}\ell} = \frac{k_{\mathrm{ps}}}{k_{\mathrm{cat}}}\rho_{\mathrm{n}\ell}. \tag{C9}$$

Based on the calculated analytical expressions for MT distributions, we can obtain the number of MTs at any position along the spindle axis. The MTs that cross the position x are those with the minus end and plus end on opposite sides of that position. Thus, the calculation for the number of MTs pointing rightward is given as

$$\begin{aligned} N_{\ell}(x) &= \int_{L/2+x}^{\infty} dl\,(n_{\mathrm{p}\ell}+\tilde{n}_{\mathrm{p}\ell}) + \int_{-L/2}^{x} dx' \int_{x}^{\infty} dx'' \\ &\quad\times\left[\rho_{\mathrm{n}\ell}(x', x''-x') + \tilde{\rho}_{\mathrm{n}\ell}(x', x''-x')\right] \\ &= \left(\frac{k_{\mathrm{p}}}{k_{\mathrm{ps}}}+\frac{k_{\mathrm{p}}}{k_{\mathrm{cat}}}\right)\exp\left(-\frac{L}{2l_0}\right)\exp\left(-\frac{x}{l_0}\right) \\ &\quad\times\left[1+\left(\frac{k_{\mathrm{n}}c}{k_{\mathrm{ps}}}+\frac{k_{\mathrm{n}}c}{k_{\mathrm{cat}}}\right)\left(\frac{L}{2}+x\right)\right]. \end{aligned} \tag{C10}$$

The distributions for MTs pointing leftward are given by substituting $x \to -x$ in Eqs. (C7), (C9), and (C10), whereas Eqs. (C6) and (C8) depend on MT length only and thus are identical for both directions.

APPENDIX D: CALCULATING THE KINETOCHORE MICROTUBULE DISTRIBUTIONS

We calculate the kinetochore-MT distributions in a steady-state limit. We also neglect the kinetochore velocity v_{kc} since it is much smaller than the MT growth velocity v_{g}. With these approximations, Eqs. (13) and (14) simplify to

$$0 = v_{\mathrm{g}}p_{\mathrm{att}}\left(1-\frac{N_{\mathrm{k}\ell}}{N_0}\right)n_{\mathrm{p}\ell}\Big|_{l=L/2+x_{\mathrm{kc}}} - k_{\mathrm{off}}N_{\mathrm{kp}\ell}, \tag{D1}$$

$$0 = v_{\mathrm{g}}p_{\mathrm{att}}\left(1-\frac{N_{\mathrm{k}\ell}}{N_0}\right)\rho_{\mathrm{n}\ell}\Big|_{x=x_{\mathrm{kc}}-l} - k_{\mathrm{off}}n_{\mathrm{kn}\ell}. \tag{D2}$$

Note that these equations describe MTs attached to the left kinetochore. These coupled algebraic equations (D1) and (D2) link the distributions of kinetochore MTs that extend from the pole and along preexisting MTs, yielding a linear relationship with a coefficient that depends on the position along the spindle:

$$n_{\mathrm{kn}\ell} = \frac{\rho_{\mathrm{n}\ell}|_{x=x_{\mathrm{kc}}-l}}{n_{\mathrm{p}\ell}|_{l=L/2+x_{\mathrm{kc}}}}N_{\mathrm{kp}\ell}. \tag{D3}$$

Inserting this result in the equation for the total number of MTs at the left kinetochore [Eq. (15)] and using the fact that $\rho_{\mathrm{n}\ell}|_{x=x_{\mathrm{kc}}-l}$ does not depend on l, it follows that

$$N_{\mathrm{k}\ell} = N_{\mathrm{kp}\ell}\left[1+\left(\frac{L}{2}-x_{\mathrm{kc}}\right)\frac{\rho_{\mathrm{n}\ell}|_{x=x_{\mathrm{kc}}-l}}{n_{\mathrm{p}\ell}|_{l=L/2+x_{\mathrm{kc}}}}\right]. \tag{D4}$$

Combining this result with Eqs. (D1) and (D2), the number of left kinetochore MTs that reach the pole is given as

$$N_{\mathrm{kp}\ell} = \frac{N_0 n_{\mathrm{p}\ell}|_{l=L/2+x_{\mathrm{kc}}}}{\frac{N_0 k_{\mathrm{off}}}{v_{\mathrm{g}}p_{\mathrm{att}}} + n_{\mathrm{p}\ell}|_{l=L/2+x_{\mathrm{kc}}} + \left(\frac{L}{2}-x_{\mathrm{kc}}\right)\rho_{\mathrm{n}\ell}|_{x=x_{\mathrm{kc}}-l}}, \tag{D5}$$

whereas the length distribution of MTs that do not reach the pole is given as

$$n_{\mathrm{kn}\ell} = \frac{N_0 \rho_{\mathrm{n}\ell}|_{x=x_{\mathrm{kc}}-l}}{\frac{N_0 k_{\mathrm{off}}}{v_{\mathrm{g}}p_{\mathrm{att}}} + n_{\mathrm{p}\ell}|_{l=L/2+x_{\mathrm{kc}}} + \left(\frac{L}{2}-x_{\mathrm{kc}}\right)\rho_{\mathrm{n}\ell}|_{x=x_{\mathrm{kc}}-l}}. \tag{D6}$$

The number of kinetochore MTs nucleated along preexisting MTs that reach position x is calculated as

$$\begin{aligned} N_{\mathrm{kn}\ell}(x) &= \int_{x_{\mathrm{kc}}-x}^{L/2+x_{\mathrm{kc}}} n_{\mathrm{kn}\ell}\,dl \\ &= \left(\frac{L}{2}+x\right)n_{\mathrm{kn}\ell}. \end{aligned} \tag{D7}$$

In particular, the total number of kinetochore MTs nucleated along preexisting MTs is given by $N_{\mathrm{kn}\ell}(x_{\mathrm{kc}})$.

The kinetochore-MT distributions on the right kinetochore follow by substituting $x \to -x$ and $x_{\mathrm{kc}} \to -x_{\mathrm{kc}}$ in Eqs. (D5)–(D7), as well as by using the right side MT distributions instead of the left.

APPENDIX E: STABILITY ANALYSIS FOR KINETOCHORES IN THE VICINITY OF THE SPINDLE EQUATOR

In order to explore the stability of the positioning of kinetochores around the spindle center, we calculate the kinetochore velocity direction in the vicinity of the spindle center. From Eq. (C10) follows a mirror symmetry with

respect to the spindle center for the probability of motor protein attachment for the left and right sides $P_\ell(x) = P_r(-x)$. Due to this symmetry, there is also a mirror symmetry for the motor protein and cross-linker numbers for the left and right sides $M_{\rm mr}(x) = M_{{\rm m}\ell}(-x)$ and $M_{\rm cr}(x) = M_{{\rm c}\ell}(-x)$. By using these symmetries to calculate the kinetochore velocity, from Eq. (13) it follows that the velocity is antisymmetric with respect to the spindle center $v_{\rm kc}(x) = -v_{\rm kc}(-x)$ and it is equal to zero at the spindle center. We calculate the kinetochore velocity in the vicinity of the spindle center, at position $x_{\rm kc} = \epsilon$, which is small compared to the typical MT length $|\epsilon| \ll l_0$. Taylor expansion of $v_{\rm kc}$ as a function of the position x at the point $x = 0$ up to the first term gives $v_{\rm kc}(\epsilon) = v'_{\rm kc}(0)\epsilon$. Here and throughout the text, the prime denotes the first derivative of a function with respect to x. By taking the first derivative of Eq. (13) at $x = 0$ and by using the mirror symmetries of the motor proteins, the cross-linkers, and the motor protein attachment probabilities we find

$$v'_{\rm kc}(0) = \frac{v_0}{\gamma_{\rm MT}}\left(\frac{f_0}{v_0}[M'_{\rm mr}(0)] + \xi_{\rm c}[M'_{\rm cr}(0)]\right) + 2\frac{v_{\rm CE0} - v_0/2}{\gamma_{\rm CE}}\frac{f_{\rm CE0}}{v_{\rm CE0}}2N_{\rm CE}P'_\ell(0). \tag{E1}$$

This equation provides straightforward information about the stability of the kinetochore positioning, where for negative values of the velocity derivative the kinetochore is at a stable position.

APPENDIX F: MOVEMENTS OF THE KINETOCHORE DUE TO KINETOCHORE MOTOR PROTEINS

In Sec. III D it was shown that the kinetochore velocity is oriented toward the center under the influence of the kinetochore motor proteins. However, it is possible to find a choice of parameters for which the kinetochore velocity is not oriented toward the center. We proceed from Eq. (E1) and calculate

$$P'_\ell = \frac{N'_\ell N_{\rm r} - N_\ell N'_{\rm r}}{(N_\ell + N_{\rm r})^2}. \tag{F1}$$

Next we substitute the expressions for N_ℓ and $N_{\rm r}$ calculated from Eq. (C10) at position $x_{\rm kc} = 0$,

$$P'_\ell = \frac{-\frac{1}{l_0} + \left(1 - \frac{L}{2l_0}\right)\left(\frac{k_{\rm n}c}{k_{\rm ps}} + \frac{k_{\rm n}c}{k_{\rm cat}}\right)}{2\left[1 + \frac{L}{2}\left(\frac{k_{\rm n}c}{k_{\rm ps}} + \frac{k_{\rm n}c}{k_{\rm cat}}\right)\right]}. \tag{F2}$$

From this equation we see that when no nucleation along preexisting MTs is present or for $l_0 < L/2$ we get $P'_\ell < 0$. In this case, if $v_{\rm CE} > v_0/2$, the contributions of kinetochore motor proteins to the force driving the movements of chromosomes are toward the center. On the other hand, if nucleation along preexisting MTs satisfies $k_n c > \frac{k_{\rm ps}k_{\rm cat}}{k_{\rm ps}+k_{\rm cat}}\frac{1}{l_0 - L/2}$ and if $l_0 > L/2$, we have $P'_\ell > 0$. In this case, if $v_{\rm CE} > v_0/2$, the contributions of kinetochore motor proteins to the force driving the movements of the chromosomes are directed toward the poles in the region around the spindle center.

[1] W. Flemming, Beitrage zur kenntniss der zelle und ihrer lebenserscheinungen: Theil II, Arch. Mikrosk. Anat. **18**, 151 (1880).

[2] L. Drüner, Studien über den mechanismus der zelltheilung, Jenaische Ztschr. Naturw. **29**, 271 (1895).

[3] R. B. Nicklas and C. A. Staehly, Chromosome micromanipulation, Chromosoma **21**, 1 (1967).

[4] R. B. Nicklas, Measurements of the force produced by the mitotic spindle in anaphase, J. Cell Biol. **97**, 542 (1983).

[5] V. Magidson, C. B. O'Connell, J. Lončarek, R. Paul, A. Mogilner, and A. Khodjakov, The spatial arrangement of chromosomes during prometaphase facilitates spindle assembly, Cell **146**, 555 (2011).

[6] N. Pavin and I. M. Tolić, Self-organization and forces in the mitotic spindle, Annu. Rev. Biophys. **45**, 279 (2016).

[7] N. Pavin and I. M. Tolić, Mechanobiology of the mitotic spindle, Dev. Cell **56**, 192 (2021).

[8] R. Kiewisz, G. Fabig, W. Conway, D. Baum, D. Needleman, and T. Müller-Reichert, Three-dimensional structure of kinetochore-fibers in human mitotic spindles, eLife **11**, e75459 (2022).

[9] T. Mitchison and M. Kirschner, Dynamic instability of microtubule growth, Nature (London) **312**, 237 (1984).

[10] A. Musacchio and A. Desai, A molecular view of kinetochore assembly and function, Biology **6**, 5 (2017).

[11] I. Hagan and M. Yanagida, Novel potential mitotic motor protein encoded by the fission yeast *cut7*$^+$ gene, Nature (London) **347**, 563 (1990).

[12] K. E. Sawin, K. LeGuellec, M. Philippe, and T. J. Mitchison, Mitotic spindle organization by a plus-end-directed microtubule motor, Nature (London) **359**, 540 (1992).

[13] D. Pellman, Two microtubule-associated proteins required for anaphase spindle movement in saccharomyces cerevisiae, J. Cell Biol. **130**, 1373 (1995).

[14] W. Jiang, G. Jimenez, N. J. Wells, T. J. Hope, G. M. Wahl, T. Hunter, and R. Fukunaga, PRC1: A human mitotic spindle-associated CDK substrate protein required for cytokinesis, Mol. Cell **2**, 877 (1998).

[15] P. Bieling, I. A. Telley, and T. Surrey, A minimal midzone protein module controls formation and length of antiparallel microtubule overlaps, Cell **142**, 420 (2010).

[16] C. Mollinari, J.-P. Kleman, W. Jiang, G. Schoehn, T. Hunter, and R. L. Margolis, PRC1 is a microtubule binding and bundling protein essential to maintain the mitotic spindle midzone, J. Cell Biol. **157**, 1175 (2002).

[17] J. Kajtez, A. Solomatina, M. Novak, B. Polak, K. Vukušić, J. Rüdiger, G. Cojoc, A. Milas, I. Š. Šestak, P. Risteski, F. Tavano, A. H. Klemm, E. Roscioli, J. Welburn, D. Cimini, M. Glunčić, N. Pavin, and I. M. Tolić, Overlap microtubules link sister k-fibres and balance the forces on bi-oriented kinetochores, Nat. Commun. **7**, 10298 (2016).

[18] H. Maiato, A. Gomes, F. Sousa, and M. Barisic, Mechanisms of chromosome congression during mitosis, Biology **6**, 13 (2017).

[19] C. L. Rieder, E. A. Davison, L. C. Jensen, L. Cassimeris, and E. D. Salmon, Oscillatory movements of monooriented chromosomes and their position relative to the spindle pole result from

the ejection properties of the aster and half-spindle., J. Cell Biol. **103**, 581 (1986).
[20] C. Rieder and E. Salmon, Motile kinetochores and polar ejection forces dictate chromosome position on the vertebrate mitotic spindle, J. Cell Biol. **124**, 223 (1994).
[21] A. S. Bajer, Functional autonomy of monopolar spindle and evidence for oscillatory movement in mitosis, J. Cell Biol. **93**, 33 (1982).
[22] A. S. Bajer and J. Mole-Bajer, *Spindle Dynamics and Chromosome Movements* (Academic, New York, 1972), Suppl. 3.
[23] S. Cai, C. B. O'Connell, A. Khodjakov, and C. E. Walczak, Chromosome congression in the absence of kinetochore fibres, Nat. Cell Biol. **11**, 832 (2009).
[24] M. Barisic, P. Aguiar, S. Geley, and H. Maiato, Kinetochore motors drive congression of peripheral polar chromosomes by overcoming random arm-ejection forces, Nat. Cell Biol. **16**, 1249 (2014).
[25] K. Vukušić and I. M. Tolić, CENP-E initiates chromosome congression by opposing aurora kinases to promote end-on microtubule attachments close to centrosomes, bioRxiv (2023), doi:10.1101/2023.10.19.563150.
[26] S. Inoué, The effect of colchicine on the microscopic and submicroscopic structure of the mitotic spindle, Exp. Cell Res. **2**, 89 (1952).
[27] D. E. Koshland, T. J. Mitchison, and M. W. Kirschner, Polewards chromosome movement driven by microtubule depolymerization *in vitro*, Nature (London) **331**, 499 (1988).
[28] M. Coue, V. A. Lombillo, and J. R. McIntosh, Microtubule depolymerization promotes particle and chromosome movement *in vitro*, J. Cell Biol. **112**, 1165 (1991).
[29] E. L. Grishchuk, M. I. Molodtsov, F. I. Ataullakhanov, and J. R. McIntosh, Force production by disassembling microtubules, Nature (London) **438**, 384 (2005).
[30] J. Stumpff, G. von Dassow, M. Wagenbach, C. Asbury, and L. Wordeman, The kinesin-8 motor Kif18A suppresses kinetochore movements to control mitotic chromosome alignment, Dev. Cell **14**, 252 (2008).
[31] V. Varga, J. Helenius, K. Tanaka, A. A. Hyman, T. U. Tanaka, and J. Howard, Yeast kinesin-8 depolymerizes microtubules in a length-dependent manner, Nat. Cell Biol. **8**, 957 (2006).
[32] R. R. West, T. Malmstrom, and J. R. McIntosh, Kinesins klp5^{+} and klp6^{+} are required for normal chromosome movement in mitosis, J. Cell Sci. **115**, 931 (2002).
[33] M. A. Garcia, N. Koonrugsa, and T. Toda, Two kinesin-like Kin I family proteins in fission yeast regulate the establishment of metaphase and the onset of anaphase A, Curr. Biol. **12**, 610 (2002).
[34] P. Risteski, D. Božan, M. Jagrić, A. Bosilj, N. Pavin, and I. M. Tolić, Length-dependent poleward flux of sister kinetochore fibers promotes chromosome alignment, Cell Rep. **40**, 111169 (2022).
[35] D. Johann, D. Goswami, and K. Kruse, Generation of stable overlaps between antiparallel filaments, Phys. Rev. Lett. **115**, 118103 (2015).
[36] M. Lera-Ramirez and F. J. Nédélec, Theory of antiparallel microtubule overlap stabilization by motors and diffusible crosslinkers, Cytoskeleton **76**, 600 (2019).
[37] F. Nédélec, Computer simulations reveal motor properties generating stable antiparallel microtubule interactions, J. Cell Biol. **158**, 1005 (2002).
[38] R. Loughlin, R. Heald, and F. Nédélec, A computational model predicts Xenopus meiotic spindle organization, J. Cell Biol. **191**, 1239 (2010).
[39] L. Winters, I. Ban, M. Prelogović, I. Kalinina, N. Pavin, and I. M. Tolić, Pivoting of microtubules driven by minus-end-directed motors leads to spindle assembly, BMC Biol. **17**, 42 (2019).
[40] A. R. Lamson, C. J. Edelmaier, M. A. Glaser, and M. D. Betterton, Theory of cytoskeletal reorganization during crosslinker-mediated mitotic spindle assembly, Biophys. J. **116**, 1719 (2019).
[41] T. E. Holy and S. Leibler, Dynamic instability of microtubules as an efficient way to search in space, Proc. Natl. Acad. Sci. USA **91**, 5682 (1994).
[42] R. Wollman, E. Cytrynbaum, J. Jones, T. Meyer, J. Scholey, and A. Mogilner, Efficient chromosome capture requires a bias in the 'search-and-capture' process during mitotic-spindle assembly, Curr. Biol. **15**, 828 (2005).
[43] R. Paul, R. Wollman, W. T. Silkworth, I. K. Nardi, D. Cimini, and A. Mogilner, Computer simulations predict that chromosome movements and rotations accelerate mitotic spindle assembly without compromising accuracy, Proc. Natl. Acad. Sci. USA **106**, 15708 (2009).
[44] I. Kalinina, A. Nandi, P. Delivani, M. R. Chacón, A. H. Klemm, D. Ramunno-Johnson, A. Krull, B. Lindner, N. Pavin, and I. M. Tolić-Nørrelykke, Pivoting of microtubules around the spindle pole accelerates kinetochore capture, Nat. Cell Biol. **15**, 82 (2013).
[45] A. V. Zaytsev and E. L. Grishchuk, Basic mechanism for biorientation of mitotic chromosomes is provided by the kinetochore geometry and indiscriminate turnover of kinetochore microtubules, Mol. Biol. Cell **26**, 3985 (2015).
[46] C. Edelmaier, A. R. Lamson, Z. R. Gergely, S. Ansari, R. Blackwell, J. R. McIntosh, M. A. Glaser, and M. D. Betterton, Mechanisms of chromosome biorientation and bipolar spindle assembly analyzed by computational modeling, eLife **9**, e48787 (2020).
[47] E. Kliuchnikov, A. Zhmurov, K. A. Marx, A. Mogilner, and V. Barsegov, CellDynaMo–stochastic reaction-diffusion-dynamics model: Application to search-and-capture process of mitotic spindle assembly, PLoS Comput. Biol. **18**, e1010165 (2022).
[48] B. L. Sprague, C. G. Pearson, P. S. Maddox, K. S. Bloom, E. Salmon, and D. J. Odde, Mechanisms of microtubule-based kinetochore positioning in the yeast metaphase spindle, Biophys. J. **84**, 3529 (2003).
[49] M. K. Gardner, C. G. Pearson, B. L. Sprague, T. R. Zarzar, K. Bloom, E. D. Salmon, and D. J. Odde, Tension-dependent regulation of microtubule dynamics at kinetochores can explain metaphase congression in yeast, Mol. Biol. Cell **16**, 3764 (2005).
[50] M. K. Gardner, D. C. Bouck, L. V. Paliulis, J. B. Meehl, E. T. O'Toole, J. Haase, A. Soubry, A. P. Joglekar, M. Winey, E. D. Salmon, K. Bloom, and D. J. Odde, Chromosome congression by kinesin-5 motor-mediated disassembly of longer kinetochore microtubules, Cell **135**, 894 (2008).
[51] H. Mary, J. Fouchard, G. Gay, C. Reyes, T. Gauthier, C. Gruget, J. Pécréaux, S. Tournier, and Y. Gachet, Fission yeast kinesin-8 controls chromosome congression independently of oscillations, J. Cell Sci. **128**, 3720 (2015).

[52] Z. R. Gergely, A. Crapo, L. E. Hough, J. R. McIntosh, and M. D. Betterton, Kinesin-8 effects on mitotic microtubule dynamics contribute to spindle function in fission yeast, Mol. Biol. Cell **27**, 3490 (2016).

[53] A. P. Joglekar and A. J. Hunt, A simple, mechanistic model for directional instability during mitotic chromosome movements, Biophys. J. **83**, 42 (2002).

[54] G. Civelekoglu-Scholey, D. Sharp, A. Mogilner, and J. Scholey, Model of chromosome motility in drosophila embryos: Adaptation of a general mechanism for rapid mitosis, Biophys. J. **90**, 3966 (2006).

[55] G. Civelekoglu-Scholey, B. He, M. Shen, X. Wan, E. Roscioli, B. Bowden, and D. Cimini, Dynamic bonds and polar ejection force distribution explain kinetochore oscillations in PtK1 cells, J. Cell Biol. **201**, 577 (2013).

[56] J. W. Armond, E. F. Harry, A. D. McAinsh, and N. J. Burroughs, Inferring the forces controlling metaphase kinetochore oscillations by reverse engineering system dynamics, PLoS Comput. Biol. **11**, e1004607 (2015).

[57] E. Kliuchnikov, K. A. Marx, A. Mogilner, and V. Barsegov, Interrelated effects of chromosome size, mechanics, number, location-orientation and polar ejection force on the spindle accuracy: A 3D computational study, Mol. Biol. Cell **34**, ar57 (2023).

[58] D. T. Miyamoto, Z. E. Perlman, K. S. Burbank, A. C. Groen, and T. J. Mitchison, The kinesin Eg5 drives poleward microtubule flux in *Xenopus laevis* egg extract spindles, J. Cell Biol. **167**, 813 (2004).

[59] I. Brust-Mascher, P. Sommi, D. K. Cheerambathur, and J. M. Scholey, Kinesin-5–dependent poleward flux and spindle length control in *Drosophila* embryo mitosis, Mol. Biol. Cell **20**, 1749 (2009).

[60] Y. Shimamoto, S. Forth, and T. M. Kapoor, Measuring pushing and braking forces generated by ensembles of kinesin-5 crosslinking two microtubules, Dev. Cell **34**, 669 (2015).

[61] M. W. Elting, M. Prakash, D. B. Udy, and S. Dumont, Mapping load-bearing in the mammalian spindle reveals local kinetochore fiber anchorage that provides mechanical isolation and redundancy, Curr. Biol. **27**, 2112 (2017).

[62] B. Akiyoshi, K. K. Sarangapani, A. F. Powers, C. R. Nelson, S. L. Reichow, H. Arellano-Santoyo, T. Gonen, J. A. Ranish, C. L. Asbury, and S. Biggins, Tension directly stabilizes reconstituted kinetochore-microtubule attachments, Nature (London) **468**, 576 (2010).

[63] F. Verde, M. Dogterom, E. Stelzer, E. Karsenti, and S. Leibler, Control of microtubule dynamics and length by cyclin A- and cyclin B-dependent kinases in xenopus egg extracts, J. Cell Biol. **118**, 1097 (1992).

[64] M. Dogterom and S. Leibler, Physical aspects of the growth and regulation of microtubule structures, Phys. Rev. Lett. **70**, 1347 (1993).

[65] K. Ishihara, K. S. Korolev, and T. J. Mitchison, Physical basis of large microtubule aster growth, eLife **5**, e19145 (2016).

[66] S. J. Klaasen, M. A. Truong, R. H. van Jaarsveld, I. Koprivec, V. Štimac, S. G. de Vries, P. Risteski, S. Kodba, K. Vukušić, K. L. de Luca, J. F. Marques, E. M. Gerrits, B. Bakker, F. Foijer, J. Kind, I. M. Tolić, S. M. A. Lens, and G. J. P. L. Kops, Nuclear chromosome locations dictate segregation error frequencies, Nature (London) **607**, 604 (2022).

[67] L. Kabeche and D. A. Compton, Cyclin A regulates kinetochore microtubules to promote faithful chromosome segregation, Nature (London) **502**, 110 (2013).

[68] J. Matković, S. Ghosh, M. Ćosić, S. Eibes, M. Barišić, N. Pavin, and I. M. Tolić, Kinetochore- and chromosome-driven transition of microtubules into bundles promotes spindle assembly, Nat. Commun. **13**, 7307 (2022).

[69] N. Yamashita, M. Morita, W. R. Legant, B.-C. Chen, E. Betzig, H. Yokota, and Y. Mimori-Kiyosue, Three-dimensional tracking of plus-tips by lattice light-sheet microscopy permits the quantification of microtubule growth trajectories within the mitotic apparatus, J. Biomed. Opt. **20**, 101206 (2015).

[70] J. G. DeLuca, Y. Dong, P. Hergert, J. Strauss, J. M. Hickey, E. D. Salmon, and B. F. McEwen, Hec1 and Nuf2 are core components of the kinetochore outer plate essential for organizing microtubule attachment sites, Mol. Biol. Cell **16**, 519 (2005).

[71] M. I. Anjur-Dietrich, C. P. Kelleher, and D. J. Needleman, Mechanical mechanisms of chromosome segregation, Cells **10**, 465 (2021).

[72] M. T. Valentine, P. M. Fordyce, T. C. Krzysiak, S. P. Gilbert, and S. M. Block, Individual dimers of the mitotic kinesin motor Eg5 step processively and support substantial loads in vitro, Nat. Cell Biol. **8**, 470 (2006).

[73] X. Yao, K. L. Anderson, and D. W. Cleveland, The microtubule-dependent motor centromere–associated protein E (CENP-E) is an integral component of kinetochore corona fibers that link centromeres to spindle microtubules, J. Cell Biol. **139**, 435 (1997).

[74] H. Yardimci, M. van Duffelen, Y. Mao, S. S. Rosenfeld, and P. R. Selvin, The mitotic kinesin CENP-E is a processive transport motor, Proc. Natl. Acad. Sci. USA **105**, 6016 (2008).

[75] Y. Du, C. A. English, and R. Ohi, The kinesin-8 Kif18A dampens microtubule plus-end dynamics, Curr. Biol. **20**, 374 (2010).

[76] J. Stumpff, Y. Du, C. A. English, Z. Maliga, M. Wagenbach, C. L. Asbury, L. Wordeman, and R. Ohi, A tethering mechanism controls the processivity and kinetochore-microtubule plus-end enrichment of the kinesin-8 Kif18A, Mol. Cell **43**, 764 (2011).

[77] E. Vladimirou, N. Mchedlishvili, I. Gasic, J. W. Armond, C. P. Samora, P. Meraldi, and A. D. McAinsh, Nonautonomous movement of chromosomes in mitosis, Dev. Cell **27**, 60 (2013).

[78] D. Cimini, B. Howell, P. Maddox, A. Khodjakov, F. Degrassi, and E. Salmon, Merotelic kinetochore orientation is a major mechanism of aneuploidy in mitotic mammalian tissue cells, J. Cell Biol. **153**, 517 (2001).

[79] G. Cojoc, E. Roscioli, L. Zhang, A. García-Ulloa, J. V. Shah, M. W. Berns, N. Pavin, D. Cimini, I. M. Tolić, and J. Gregan, Laser microsurgery reveals conserved viscoelastic behavior of the kinetochore, J. Cell Biol. **212**, 767 (2016).

[80] R. B. Nicklas, How cells get the right chromosomes, Science **275**, 632 (1997).

[81] S. Biggins, F. F. Severin, N. Bhalla, I. Sassoon, A. A. Hyman, and A. W. Murray, The conserved protein kinase Ipl1 regulates microtubule binding to kinetochores in budding yeast, Genes Dev. **13**, 532 (1999).

[82] T. U. Tanaka, N. Rachidi, C. Janke, G. Pereira, M. Galova, E. Schiebel, M. Stark, and K. Nasmyth, Evidence that the Ipl1-Sli15 (Aurora kinase-INCENP) complex promotes chromosome bi-orientation by altering kinetochore-spindle pole connections, Cell **108**, 317 (2002).

[83] A. K. de Regt, C. J. Clark, C. L. Asbury, and S. Biggins, Tension can directly suppress Aurora B kinase-triggered release of kinetochore-microtubule attachments, Nat. Commun. **13**, 2152 (2022).